AGU PUBLICATIONS

JGR

Journal of Geophysical Research: Solid Earth

RESEARCH ARTICLE

10.1002/2015JB012595

Key Points:
- Seismic rate density
- Time-independent probability of earthquake occurrence
- Time-dependent probability with inclusion of stress transfer

Supporting Information:
- Supporting Information S1
- Table S1
- Table S2
- Table S3
- Table S4
- Table S5
- Table S6

Correspondence to:
M. Murru,
maura.murru@ingv.it

Citation:
Murru, M., A. Akinci, G. Falcone, S. Pucci, R. Console, and T. Parsons (2016), $M \geq 7$ earthquake rupture forecast and time-dependent probability for the sea of Marmara region, Turkey, *J. Geophys. Res. Solid Earth*, *121*, doi:10.1002/2015JB012595.

Received 12 OCT 2015
Accepted 28 MAR 2016
Accepted article online 2 APR 2016

$M \geq 7$ earthquake rupture forecast and time-dependent probability for the sea of Marmara region, Turkey

M. Murru[1], A. Akinci[1], G. Falcone[1], S. Pucci[1], R. Console[1,2], and T. Parsons[3]

[1]Istituto Nazionale di Geofisica e Vulcanologia, Rome, Italy, [2]Center of Integrated Geomorphology for the Mediterranean Area, Potenza, Italy, [3]U.S. Geological Survey, Menlo Park, California, USA

Abstract We forecast time-independent and time-dependent earthquake ruptures in the Marmara region of Turkey for the next 30 years using a new fault segmentation model. We also augment time-dependent Brownian passage time (BPT) probability with static Coulomb stress changes (ΔCFF) from interacting faults. We calculate $M_w > 6.5$ probability from 26 individual fault sources in the Marmara region. We also consider a multisegment rupture model that allows higher-magnitude ruptures over some segments of the northern branch of the North Anatolian Fault Zone beneath the Marmara Sea. A total of 10 different $M_w = 7.0$ to $M_w = 8.0$ multisegment ruptures are combined with the other regional faults at rates that balance the overall moment accumulation. We use Gaussian random distributions to treat parameter uncertainties (e.g., aperiodicity, maximum expected magnitude, slip rate, and consequently mean recurrence time) of the statistical distributions associated with each fault source. We then estimate uncertainties of the 30 year probability values for the next characteristic event obtained from three different models (Poisson, BPT, and BPT + ΔCFF) using a Monte Carlo procedure. The Gerede fault segment located at the eastern end of the Marmara region shows the highest 30 year probability, with a Poisson value of 29% and a time-dependent interaction probability of 48%. We find an aggregated 30 year Poisson probability of $M > 7.3$ earthquakes at Istanbul of 35%, which increases to 47% if time dependence and stress transfer are considered. We calculate a twofold probability gain (ratio time dependent to time independent) on the southern strands of the North Anatolian Fault Zone.

1. Introduction

The devastating 17 August 1999 Izmit (M_w7.4) and 12 November 1999 Düzce (M_w7.1) earthquakes in the Marmara region of Turkey ruptured adjacent segments of the North Anatolian Fault Zone (NAFZ) [*Barka*, 1999; *Barka et al*., 2002; *Utkucu et al*., 2003]. This fault zone slices through Northern Turkey for more than 1500 km, accommodating ~25 mm/yr of right-lateral motion between the Anatolia microplate and the Eurasian plate [i.e., *Reilinger et al*., 2006]. It has generated more than 10 $M \geq 6.7$ earthquakes during the 20th century, often with tragic results (Table 1). A pair of earthquakes broke much of the NAFZ under the Sea of Marmara in 1766, but they left a 150 km long unruptured section in the immediate vicinity of the broader Istanbul metropolitan area ("Marmara seismic gap") where a major earthquake with a magnitude of up to 7.4 is expected for the near future. Recent studies confirm that present-day tectonic loading, seismic slip deficit, and thus the probability of having a large earthquake appear to be particularly high along the segments located in the Marmara Sea, southwest of Istanbul [*Hubert-Ferrari et al*., 2000; *Armijo et al*., 2005; *Pondard et al*., 2007; *Bohnhoff et al*., 2013].

Stress transfer from the M_w7.4 Izmit earthquake of 1999 may have exacerbated the problem; *Parsons et al*. [2000] calculated a combined interaction probability for faults within 50 km of Istanbul to be 62 ± 15% (with quoted uncertainties at 1σ) to cause strong shaking (Modified Mercalli Intensity scale ≥ VIII) for the period May 2000 to May 2030. New high-resolution images of the Marmara seafloor [*Le Pichon et al*., 2001; *Armijo et al*., 2002, 2005] enabled detailed fault mapping and updated 30 year earthquake probability calculations (2004–2034) for the Sea of Marmara region and the city of Istanbul (51 ± 18% regional interaction probability, 39 ± 18% for Istanbul) [*Parsons*, 2004].

The Marmara region is confronted by a real earthquake threat, and the need for accurate seismic hazard assessments has become progressively more important [*Atakan et al*., 2002; *Erdik et al*., 2004; *Kalkan et al*., 2009; *Gülerce and Ocak*, 2013].

In this study, we propose a fault segmentation model based on new knowledge of the NAFZ configuration, and by integrating the geometrical parameters of each fault segment with seismological data and fault slip rate estimates [e.g., *Armijo et al*., 2002; *Hergert and Heidbach*, 2010]. As long as the fault geometry and tectonic

Table 1. Fault Parameters Used in the Modeling[a]

#	Fault Name	Kin	Magnitude Source 50th Percentile	Strike-Slip Rate (mm/yr)	Dip-Slip Rate (mm/yr)	L (km)	H (km)	W (km) (1σ)
1	Izmit-S3	SS	7.6	20 ± 2 **(1; 2)**	0 ± 1 **(3)**	158 **(4; 5; 6)**	15 ± 2.0	15.0 ± 1.0
2	Çınarcık	SS	7.0	14 ± 2 **(2; 10)**	−4 ± 2 **(2; 10)**	44 **(11; 12; 13; 14; 15)**	15 ± 2.0	15.0 ± 0.9
3	South Çınarcık	N	7.2	3 ± 1 **(10)**	−4 ± 2 **(10)**	48 **(12; 13; 14; 17)**	15 ± 2.0	16.6 ± 1.1
4	Central Marmara	SS	7.1	18 ± 2 **(1; 10)**	0 ± 1 **(3; 10)**	49 **(12; 13; 14)**	15 ± 2.0	15.1 ± 0.9
5	West Marmara	SS	7.2	18 ± 2 **(1; 10)**	−1 ± 1 **(3; 10; 19)**	61 **(11; 12)**	15 ± 2.0	15.4 ± 1.0
6	Ganos	SS	7.3	19 ± 2 **(1; 2; 10; 21; 22)**	0 ± 1 **(3; 10)**	74 **(21; 23)**	15 ± 2.0	15.6 ± 1.0
7	North Saros	SS	7.1	10 ± 2 **(1; 25)**	−2 ± 1 **(3; 19)**	46 **(26)**	15 ± 2.0	15.6 ± 1.0
8	South Saros	SS	7.1	10 ± 2 **(1; 3; 25)**	−2 ± 1 **(3; 19)**	45 **(26)**	15 ± 2.0	15.6 ± 1.0
9	Mudurnu	SS	7.2	10 ± 2 **(1; 3; 19)**	1 ± 1 **(19)**	70 **(27; 28; 29)**	15 ± 2.0	15.0 ± 0.9
10	Abant	SS	7.1	10 ± 2 **(1; 3; 19; 32)**	1 ± 1 **(19)**	55 **(27; 28)**	15 ± 2.0	15.0 ± 0.0
11	Düzce-S1	SS	7.1	15 ± 3 **(1; 34)**	0 ± 1 **(3)**	42 **(35)**	15 ± 2.0	15.7 ± 1.0
12	Gerede	SS	7.1	24 ± 1 **(1; 3; 19; 32)**	6 ± 1 **(3; 19)**	165 **(28; 37)**	15 ± 2.0	15.1 ± 1.0
13	Geyve	N	7.1	5 ± 2 **(1; 3)**	−11 ± 4 **(3; 19)**	49 **(38; 40)**	15 ± 2.0	15.3 ± 1.0
14	Iznik	N	7.1	4 ± 1 **(1; 3; 10)**	−11 ± 4 **(3; 19)**	74 **(38; 40; 43)**	15 ± 2.0	15.4 ± 1.0
15	Yenisehir	N	7.1	3 ± 1 **(1; 19)**	−7 ± 2 **(3; 19)**	40 **(38; 42)**	15 ± 2.0	15.4 ± 1.0
16	Gemlik	SS	7.1	4 ± 1 **(1; 2; 25)**	0 ± 1 **(10)**	47 **(42; 43; 44)**	15 ± 2.0	15.4 ± 1.0
17	Bursa	N	7.1	3 ± 1 **(1; 3)**	−6 ± 4 **(3; 45)**	67 **(45)**	15 ± 2.0	15.2 ± 1.0
18	South Marmara	SS	7.1	3 ± 1 **(1; 10;47)**	0 ± 1 **(10)**	83 **(44; 47)**	15 ± 2.0	15.3 ± 1.0
19	Kemalpasa	N	7.1	4 ± 3 **(1; 3; 19; 45)**	−8 ± 3 **(3; 19)**	41 **(45)**	15 ± 2.0	15.3 ± 0.9
20	Manyas	N	7.1	3±2 **(1; 3; 19; 45)**	−8 ± 3 **(19; 3; 45)**	55 **(45)**	15 ± 2.0	15.3 ± 0.9
21	Bandirma	SS	7.2	3 ± 1 **(3)**		41 **(28; 38; 42)**	15 ± 2.0	16.1 ± 1.0
22	Gönen	SS	7.2	6 ± 3 **(1; 3; 19; 45; 46)**	−1 ± 3 **(3; 45)**	50 **(46)**	15 ± 2.0	16.0 ± 1.0
23	Biga	SS	7.2	2 ± 1 **(1; 3; 10)**	0 ± 1 **(10)**	57 **(28; 38; 42)**	15 ± 2.0	16.1 ± 1.0
24	Pazarkoy	SS	7.2	3±1 **(1; 19)**	−1 ± 3 **(3)**	54 **(28; 38; 42)**	15 ± 2.0	16.0 ± 1.1
25	Can	SS	7.2	3 ± 1 **(1)**		53 **(28; 38; 42)**	15 ± 2.0	16.0 ± 1.0
26	Ezine	SS	7.2	2 ± 1 **(1; 3)**		56 **(28; 38; 42)**	15 ± 2.0	16.0 ± 0.9

[a]Kinematics (SS = strike slip; N = normal); computed magnitude, strike and dip-slip rate; length (L); depth (H); width (W); focal mechanism; last and penultimate events ages with their maximum expected magnitude (M_S), computed by instrumental or historical data, otherwise by fault geometry [*Wells and Coppersmith*, 1994]. Reference numbers refer to **(1)** *Flerit et al.* [2003], **(2)** *Ergintav et al.* [2014], **(3)** *Meade et al.* [2002], **(4)** *Barka* [1999], **(5)** *Dolu et al.* [2007], **(6)** *Rockwell et al.* [2002], **(7)** *Tibi et al.* [2001], **(8)** *Klinger et al.* [2003], **(9)** *Parson* [2004], **(10)** *Hergert and Heidbach* [2010], **(11)** *Armijo et al.* [2002], **(12)** *Le Pichon et al.* [2001, 2003], **(13)** *Carton et al.* [2007], **(14)** *Laigle et al.* [2008], **(15)** *Bulut et al.* [2009], **(16)** *Ambraseys* [2002], **(17)** *Armijo et al.* [2002, 2005]; **(18)** *Taymaz et al.* [1991] and *McKenzie* [1978]; **(19)** *Reilinger et al.* [2006], **(20)** *Guidoboni and Comastri* [2005], **(21)** *Meghraoui et al.* [2012] and *Aksoy et al.* [2010], **(22)** *Motagh et al.* [2007], **(23)** *Altunel et al.* [2004]; **(24)** *Rockwell et al.* [2001], **(25)** *Gasperini et al.* [2011], **(26)** *Yaltirak* [2002] and *McNeill et al.* [2004], **(27)** *Ambraseys and Jackson* [1998], **(28)** *Barka* [1996], **(29)** *Ambraseys and Zatopek* [1969], **(30)** *Canitez* [1972], **(31)** *Palyvos et al.* [2007], **(32)** *Straub et al.* [1997], **(33)** *Ambraseys* [1970], **(34)** *Pucci et al.* [2008], **(35)** *Pucci et al.* [2007], **(36)** *Pantosti et al.* [2008], **(37)** *Kondo et al.* [2010], **(38)** *Barka and Kadinsky-Cade* [1988], **(39)** *Ketin* [1969], **(40)** *Doğan et al.* [2015], **(41)** *Guidoboni et al.* [1994], **(42)** *Saroglu et al.* [1992], **(43)** *Barka and Kuscu* [1996], **(44)** *Kuşçu et al.* [2009], **(45)** *Selim and Tüysüz* [2013] and *Selim et al.* [2013], **(46)** *Kürçer et al.* [2008], and **(47)** *Kurtuluş and Canbay* [2007] and *Vardar et al.* [2014].

interpretations of the Marmara Sea region are subject to interpretation [*Aksu et al.*, 2000; *Imren et al.*, 2001; *Le Pichon et al.*, 2001; *Armijo et al.*, 2002, 2005; *Pondard et al.*, 2007], we integrate as many observations as possible to constrain earthquake probabilities for the Marmara region taking into account three major strands: the northern (NNAF) branch, which enters the Marmara Sea, and the central (CNAF) and southern (SNAF) branches, which run onland, south of the Marmara region.

The regularity of earthquake ruptures can be affected by interaction between neighboring faults, which modifies the probability of future events [e.g., *Parsons*, 2005]. We incorporate these effects by applying two probability models, BPT and BPT together with a Coulomb stress transfer (BPT + ΔCFF), that consider fault interactions, to assess the occurrence probability of future earthquakes in the next 30 years starting on 1 January 2015. The time-independent Poisson model is also considered in the probability computation. For a comparison among the results obtained from the three different models, we consider the 16th, 50th, and 84th percentiles of a Monte Carlo distribution of probability calculations developed by varying parameter uncertainties and constrained by moment balancing against the measured relative block motion between the Anatolian and Eurasian plates.

It is important to underline that in this paper we focus only on the first component of the probabilistic seismic hazard assessment (PSHA), as it defines an earthquake rupture forecast and their probabilities and does not deal with the relative ground motions produced by the earthquake rupture. The second part, which includes an estimate of occurrence probabilities combined with estimates of ground shaking, will be examined in a future study in the same region, and especially for the city of Istanbul. The possibility that a seismic gap close

Table 1. (continued)

Strike (°)	Dip (°)	Rake (°)	Last Event (AD)	Last Event (M_s)	Penultimate Event (AD)	Penultimate Event (M_s)	T elapsed (yrs)
268	84	180	17/08/1999 **(7)**	7.4 (M_w)	25/05/1719 **(8; 9)**	7.4	16
116	88	196	10/07/1894 **(16)**	7.3	25/10/989 **(16)**	7.2	121
283	65	233	18/09/1963 **(18)**	6.4	02/09/1754 **(9;16)**	6.8–7.0	52
83	84	180	22/05/1766 **(16)**	7.1	10/09/1509 **(16)**	7.2	249
84	78	183	18/10/1343 **(16; 20)**	7.0	23/09/1063 **(16; 20)**	7.4	672
246	75	180	09/08/1912 **(9; 16; 24; 21)**	7.4	05/08/1766 **(9; 16; 24; 21)**	7.4	103
76	75	191	13/09/1912 **(16)**	6.8	17/02/1659 **(16)**	7.2	103
241	75	191	21/08/1859 **(16)**	6.8	18/05/1625 **(16)**	7.1	156
291	85	174	22/07/1967 **(29; 30)**	7.2	00/00/1600 **(31)**	?	48
236	85	174	26/05/1957 **(27; 33)**	7.2	17/08/1668 **(27; 33)**	7.9	58
262	73	180	12/11/1999 **(7)**	7.1 (M_w)	25/05/1719 **(36)**	7.4	16
261	85	166	01/02/1944 **(18; 27; 33; 38; 39)**	7.4	17/08/1668 **(27; 33)**	7.9	71
256	78	246	01/06/1296 **(16)**	7.0	11/10/368 **(16; 27; 41)**	6.8	719
259	78	250	15/03/1419 **(16; 20; 27)**	7.2	00/00/121 **(16; 41)**	7.4	596
237	78	247	01/09/1065 **(16; 20)**	6.8			950
271	78	180	11/04/1855 **(16; 20; 27)**	6.6			160
261	80	243	00/00/1143 **(20)**	?			872
268	78	180	10/05/1556 **(16)**	7.2	26/10/740 **(16)**	7.1	459
254	78	243	28/02/1855 **(27; 38)**	7.1	-		160
282	78	249	10/06/1964 **(16; 18; 27)**	6.9	00/11/368 **(16)**	6.8	51
231	70	180	10/11/123 **(16)**	7.0	-		1892
243	70	189	18/03/1953 **(16; 18; 27; 20; 38)**	7.1	00/00/1440 **(46)**	?	62
241	70	180	03/03/1969 **(18)**	6.0	7/04/460 **(16; 27; 41)**	6.9	46
60	70	198	06/10/1944 **(16)**	6.8	00/00/160 **(16)**	7.1	71
241	70	180	06/03/1737 (16)	7,0	00/00/155 **(16; 27)**	6.5	278
238	70	180	14/02/1672 **(16)**	7.0			343

to failure exists near Istanbul motivated the MARSite European Integrated Project that is aimed at mitigating seismic risk. This study contributes an earthquake rupture forecast that includes multisegment ruptures up to $M_w \sim 8.0$ that could affect Istanbul and surroundings.

2. Tectonic Setting

The east-west trending, right-lateral NAFZ extends 1500 km from the northern Aegean Sea to the Karliova triple junction in Eastern Turkey [*Barka*, 1992; *Sengör et al*., 2005; *McKenzie*, 1972; *Saroglu et al*., 1992] (inset of Figure 1). The eastern NAFZ is essentially a single trace [*Barka*, 1996] but becomes more complex to the west as it enters the Sea of Marmara region, splaying into different fault segments, ranging from 40 to 150 km long (see Figure 1 and Table 1 for detailed references). West of the town of Bolu, the Gerede segment divides into two main strands, the Düzce and Mudurnu fault segments, and farther west, it splays again into three major strands, the northern (NNAF) branch, which enters the Marmara Sea, and the central (CNAF) and southern (SNAF) branches, which run onland, south of it (Figure 1).

The NNAF strand forms a major transtensional NW-SE right bend under the Sea of Marmara at the Çınarcık trough. The fault trace follows the northern margin of the Marmara Sea and connects the complex Central Marmara and Tekirdağ pull-apart basins, before merging into the NE-SW striking Ganos fault on land. Finally, this branch exits into the Aegean Sea through the Saros Gulf [*Wong et al*., 1995; *Armijo et al*., 1999, 2002; *Okay et al*., 1999; *Le Pichon et al*., 2001; *Yaltirak*, 2002; *McNeill et al*., 2004]. In contrast with the NNAF, the central (CNAF) and southern (SNAF) traces run south of the Marmara Sea and bound several Quaternary-aged basins.

Regional GPS networks measured present-day strain rates in the northern part of the Anatolian block at ~23 ± 3 mm/yr, with vectors oriented WNW in the easternmost region, E-W in the center, and SW in the Aegean, which indicates that most of the present-day strain is accommodated along the northern fault strand at the Marmara Sea [*McClusky et al*., 2000; *Meade et al*., 2002; *Reilinger et al*., 1997, 2006; *Hergert and Heidbach*, 2010; *Hergert et al*., 2011]. The NNAF is the most active with right-lateral slip rates of 14–24 mm/yr. The CNAF branch shows about 5 mm/yr of right-lateral deformation distributed along several fault strands. The oblique right-lateral SNAF strand accommodates 2–6 mm/yr of dextral slip and up to 8 mm/yr of dip slip [*Meade et al*., 2002;

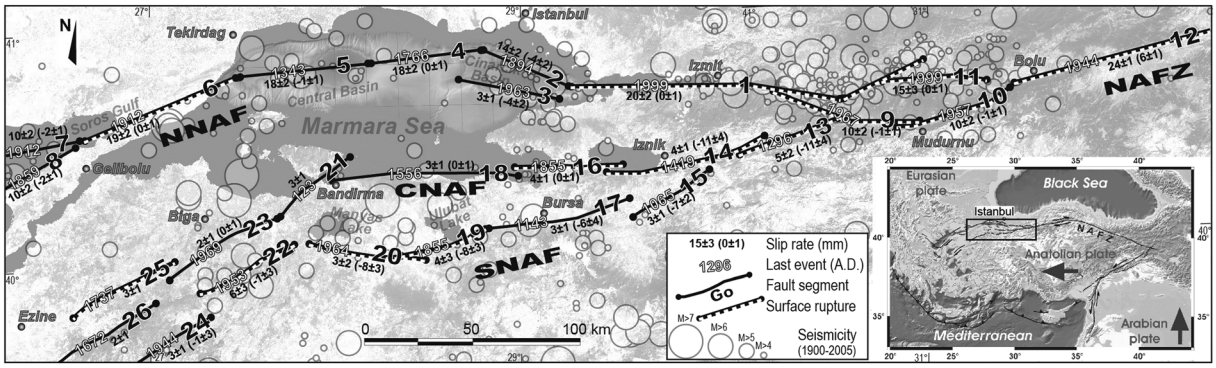

Figure 1. Fault segmentation model and the seismic activity with $M > 4.0$ from 1 January 1900 to 31 December 2006 for the Marmara region. The slip rates along the strike and dip are also shown. The inset shows some segments of the North Anatolian Fault, to the south of Istanbul. The black numbers refer to the fault names as in Table 1.

Selim et al., 2013]. Thus, the various NAF strands reveal slip partitioning, combining primary right-lateral and secondary vertical motions [*Flerit et al*., 2003, 2004; *Woodcock and Fischer*, 1986; *Pantosti et al*., 2008; *Pucci et al*., 2008].

It is possible to balance seismic strain rate released by historical and instrumental seismicity against the geodetic strain rate [*Parsons*, 2004], although alternative interpretations suggest significant aseismic creep on the central NAF [*Ergintav et al*., 2014]. This controversy results from uncertainty in locating historical earthquakes through observed intensities versus interpreting GPS transects that are necessarily incomplete because of the lacking measurements in the Marmara Sea offshore. We adopt a conservative approach of assuming complete fault coupling since the spatial and temporal resolution of the existing seismic observations does not allow us to accurately distinguish the differences between locked and creeping segments in the NAFZ [e.g., *WGCEP (Working Group on California Earthquake Probabilities*), 1995, 2003, 2008; *Field et al*., 2009, 2014]. Efforts on the high-resolution seismic networking (borehole based) in the Marmara Sea may provide better insights into the behavior of the faults with seismic earthquake gap and detect possible creeping processes impeding the occurrence of large earthquakes.

3. Historical Seismicity

Seismicity in the NAFZ is characterized by large ($M > 7$) right-lateral strike-slip earthquakes [*McKenzie*, 1972; *Reinecker et al*., 2004] (see http://www.world-stress-map.org; Table 2 and Figure 1). During the 20th century, the North Anatolian Fault produced a sequential westward progression of $M_w > 6.7$ earthquakes along the fault [*Ambraseys*, 1970; *Barka*, 1996; *Stein et al*., 1997]. The only significant portion of the NNAF that has not ruptured in the past 200 years lies submerged beneath the Marmara Sea. However, this potential seismic gap has produced large historical earthquakes and may thus be close to failure [*Hubert-Ferrari et al*., 2000; *King et al*., 2001; *Tibi et al*., 2001; *Rockwell et al*., 2001; *Ambraseys*, 2002; *Meghraoui et al*., 2012; *Aksoy et al*., 2010].

Table 2. Historical Earthquakes in the Sea of Marmara Region During the Past ~400 Years

M	Date
6.4	18 Sep 1964
7.3	10 Jul 1894
7.6	5 Aug 1766
7.1	22 May 1766
6.9	2 Sep 1754
7.2	10 Sep 1509
7.2	12 Nov 1999
7.4	17 Aug 1999
7.3	9 Aug 1912
6.0	3 Mar 1969
6.6	11 Apr 1855
7.0	6 Mar 1737
7.0	14 Feb 1672
6.9	10 Jun 1964
7.1	18 Mar 1953
6.8	6 Oct 1944
7.1	28 Feb 1855

Although the CNAF and SNAF strands have lower slip rates with respect to the NNAF, several historical and instrumental earthquakes (up to M_s7.2) can be related to specific segments that produced remarkable surface ruptures in the past and that threaten highly populated towns such as Bursa, Iznik, and Biga [*McKenzie*, 1978; *Barka and Kadinsky-Cade*, 1988; *Taymaz et al*., 1991; *Guidoboni et al*., 1994; *Ambraseys and Jackson*, 1998; *Ambraseys*, 2002; *Guidoboni and Comastri*, 2005; *Kürçer et al*., 2008] (Table 1 and Figure 1).

4. Segmentation Model

Segmenting a fault zone and assigning historical earthquakes to particular fault segments represent major assumptions that are subject to unquantifiable forecast errors, as segment boundaries and historic earthquake locations are highly dependent on the input data used and the assumptions made. Segment lengths control the magnitude distribution, and historical earthquake locations impact the time elapsed since the last rupture of a given fault segment.

The segment model defined here was based on the most detailed fault traces of the NAFZ branches available in the literature (Figure 1), and on the basis of their geometrical and structural arrangement when expressed at the surface (for details, see Chapter S1 in the supporting information). Segmentation of the NNAF beneath the Marmara Sea is especially difficult because the fault traces are not directly observable [*Aksu et al*., 2000; *Imren et al*., 2001; *Le Pichon et al*., 2001; *Armijo et al*., 2002, 2005; *Pondard et al*., 2007]. These segments are bounded by geometric fault complexities and discontinuities (e.g., jogs and fault bends) that act as barriers to rupture propagation [*Segall and Pollard*, 1980; *Barka and Kadinsky-Cade*, 1988; *Wesnousky*, 1988; *Lettis et al*., 2002; *An*, 1997]. Where possible, the reconstruction of the fault traces and boundaries at the surface is informed by seismotectonic studies of recent earthquakes (e.g., 1999 Izmit and Düzce seismic sequence) [*Gülen et al*., 2002; *Barka et al*., 2002; *Bohnhoff et al*., 2006; *Bulut et al*., 2007; *Pucci et al*., 2007; *Stierle et al*., 2014] and historical surface ruptures [*Ambraseys and Jackson*, 1998].

There is an ongoing debate about the magnitude-frequency distribution of large earthquakes on individual faults [e.g., *Schwartz and Coppersmith*, 1984; *Wesnousky*, 1994; *Stein and Newman*, 2004; *Page et al*., 2011; *Page and Felzer*, 2015]. We therefore develop a primarily characteristic earthquake rate model but also carry an alternative model that allows multisegment ruptures [e.g., *Field et al*., 2014] on the NNAF crossing the Sea of Marmara based on the possibility that occasional very large ruptures could bypass geometric fault complexities and discontinuities [e.g., *Le Pichon et al*., 2001, 2003]. This possibility is supported by the occurrence of historically documented $M \sim 8$ earthquakes along the NAFZ, east of the Marmara region (e.g., 1046 $M \sim 7.8$, 1668 $M \sim 7.9$, and 1939 $M \sim 7.9$) [*Ambraseys and Finkel,* 1995; *Ambraseys and Jackson*, 1998; *Kondorskaya and Ulomov*, 1999; *Zabcı et al*., 2011]. We therefore segment the faults (based on geologic information) at lengths near the minimum magnitude of our forecast ($M_w \sim 7.0$). Also, we allow multisegment ruptures, up to $M_w \sim 8.0$, as occurred during the 1766 events when the Central Marmara (#4) and West Marmara (#5) segments ruptured simultaneously [*Parsons et al*., 2000; *Hubert-Ferrari et al*., 2000]. This evidence reinforces the possibility that other multifault ruptures can occur in the Marmara Sea region. We include multisegment ruptures because at this time, there is no conclusive evidence proving that these ruptures cannot occur. Therefore, a comprehensive rupture forecast must include improbable but not impossible very large earthquakes. Moreover, our observation time is too short to have a complete record of infrequent, long-recurrence time earthquakes in the study region. We thus apply an earthquake simulator that can span much longer periods to produce long histories of simulated fault system characteristics and earthquake catalogs.

We adopt the fault geometry proposed by *Armijo et al*. [2002] in the Marmara Sea region because it produces the best match to the observed Marmara Sea basin morphology and geology [*Flerit et al*., 2003; *Muller and Aydin*, 2005; *Carton et al*., 2007; *Pondard et al*., 2007]. This model results in a more conservative approach because it includes more active faults. Changes in the NAFZ strike cause fault segments to evolve their kinematics from transtensive to transpressive. The largest geometrical complexity is the releasing double bend formed at the eastern Marmara Sea by the steeply dipping Çınarcık fault, which presents an important normal component. The submarine morphology [*Armijo et al*., 2005; *Laigle et al*., 2008] shows evident fault scarps beneath the Sea of Marmara that correspond to the 1912 and probably August 1766 earthquakes, as well as a new active fault showing a large submarine fault break south of the Çınarcık basin (South Çınarcık fault). The remaining surface fault traces and kinematics of the model (the CNAF and SNAF strands) are compiled from geologic mapping [*Barka and Kadinsky-Cade*, 1988; *Saroglu et al*., 1992; *Barka*, 1996; *Barka and Kuscu*, 1996; *Kurtuluş and Canbay*, 2007; *Kürçer et al*., 2008; *Kuşçu et al*., 2009; *Selim and Tüysüz,* 2013; *Selim et al*., 2013; *Vardar et al*., 2014].

The maximum seismogenic depth is assumed to be 10–15 km on the basis of the locking depth suggested by mechanical best fit modeling of GPS data [*Flerit et al*., 2003] and by the depth extent of instrumental seismicity [*Taymaz et al*., 1991; *Gürbüz et al*., 2000; *Özalaybey et al*., 2002; *Örgülü and Aktar*, 2001; *Pınar et al*., 2003].

All segments are assumed to be near vertical with right-lateral slip as suggested by geological, seismological, and GPS data. Along the NNAF, only the South Çınarcık (#3) is considered to have an important dip-slip

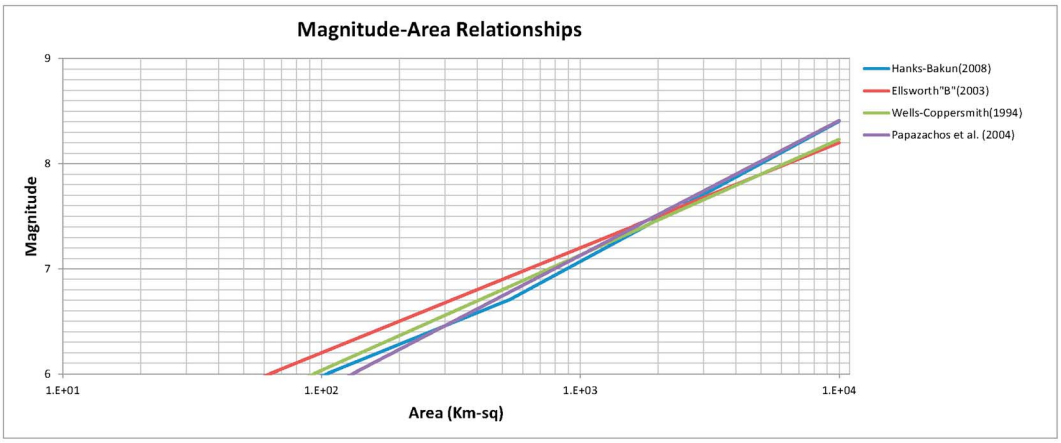

Figure 2. The magnitude-area relationships tested in the paper for the Marmara Sea region.

component based on seismological data [*McKenzie*, 1978; *Taymaz et al*., 1991]. Faults associated with a releasing bend along the CNAF and SNAF (# 13, 14, 15, 17, 19, and 20 in Figure 1 and Table 1) have a considerable normal component as interpreted from GPS data [*Meade et al*., 2002; *Reilinger et al*., 2006; *Hergert and Heidbach*, 2010; *Ergintav et al*., 2014].

We integrate geometrical and behavioral characteristics by introducing earthquake magnitude and slip rates for each fault within the segmentation model. The association of historical and instrumental earthquakes with the segmentation proposed for the three strands of the North Anatolian Fault in the Marmara region, shown in Figure 1, is given in Table 1. In addition, the maximum expected earthquake magnitude, the elapsed time since the last event, and the horizontal and vertical component of the slip rates are assigned for each fault segment. The rake values for each source were determined from the horizontal and vertical components of the slip rates and dip angles. The maximum expected magnitude is assigned on the basis of the implied rupture area for both single and multisegment ruptures (section 5.1). The magnitude is calculated by testing different empirically derived magnitude-area relationships, like *Hanks and Bakun* [2008, equations 3 and 4], *Wells and Coppersmith* [1994, equation in Table 2A for all faulting types], *Ellsworth* "B" [*WGCEP*, 2003, equation 4.5], and *Papazachos et al.* [2004, equation 8]. Figure 2 compares the rupture area of our data set with the different cited relationships, showing a difference in magnitude within the order of 0.1. Considering this low difference, we choose the *Ellsworth* "B" relation ($M_w = \log(A) + 4.2$, *WGCEP* [2003]). On the basis of this relationship, a further constraint for the segment area is given by the magnitude of the assigned historical earthquakes. Similarly, *Field et al.* [2014, Figure 12] through a consensus process could not identify a preferred magnitude-area relation and gave equal weight to *Hanks and Bakun* [2008], *Ellsworth* "B" [*WGCEP*, 2003], and *Shaw* [2009, 2013].

The deformation rates produced by the three strands of the NAFZ in the Marmara region are mostly derived from GPS studies [*Meade et al*., 2002; *Reilinger et al*., 2006; *Hergert and Heidbach*, 2010; *Ergintav et al*., 2014]. A detailed study of individual segments from both interferometric synthetic aperture radar and geological investigations provides slip rates along the NNAF strand [*Motagh et al*., 2007; *Pucci et al*., 2008; *Aksoy et al*., 2010; *Gasperini et al*., 2011; *Meghraoui et al*., 2012]. We used the results of the best fit mechanical models [*Flerit et al*., 2003; *Armijo et al*., 2002] that match the *Straub et al*. [1997] data for NNAF fault segments with unknown slip rates. Along the CNAF and SNAF strands, a few detailed studies of individual segments provide geological slip rates [*Gasperini et al*., 2011; *Selim et al*., 2013]. Here, since *Armijo et al*. [2002] and *Flerit et al*. [2003] model the CNAF and SNAF strands as a single discontinuity, we split its velocity. The proportion of the slip between the two southern strands is based on conclusions made by *Straub et al*. [1997], with the CNAF being slightly faster (~4–5 mm/yr) than the SNAF (~2–3 mm/yr).

5. Determining Earthquake Recurrence Rates

A simple spring-mass model proposed by *Reid* [1911] in his pioneering work has been the most popular idea adopted so far for modeling earthquake occurrence on long timescales. This idea led to the development of the concepts of seismic gap [*Mogi*, 1968] and the characteristic earthquake [*Schwartz and Coppersmith*, 1984;

Nishenko and Buland, 1987; *Wesnousky*, 1994], where earthquakes recur quasi-periodically on identified fault segments. The characteristic earthquake rupture model is supported by paleoseismological observations [*Schwartz and Coppersmith*, 1984; *Wesnousky*, 1994; *Hecker and Abrahamson*, 2004] and can greatly simplify earthquake rupture forecasting. If the same event has occurred repeatedly in the past, then there is implied predictability. In this case, an earthquake of the same magnitude recurs with a constant interval. This probabilistic approach for forecasting the time of the next earthquake on a specific fault segment was initially proposed by *Utsu* [1972a, 1972b], *Rikitake* [1974], and *Hagiwara* [1974].

Renewal models that describe main shock seismic cycles, such as the Brownian Passage Time (BPT) model [*Kagan and Knopoff*, 1987; *Matthews et al*., 2002], are associated with the hypothesis of characteristic earthquake and are easy to adopt. The quasi-periodic (mostly BPT-type) hypothesis of characteristic earthquake occurrence on specific faults has been considered and widely used in some regions of moderate to high seismic activity like in the San Francisco Bay region [e.g., *WGCEP*, 2003], as well as in Italy [*Akinci et al*., 2009, 2010]. Assumptions concerning the recurrence time distribution are still an open question in part because of the effect of fault interactions.

The geodetically measured cumulative strain across the plate boundary between Anatolia and Eurasia is an independent constraint on determining earthquake rate models (often referred to as moment balancing [e.g., *Field et al*., 2014]). We therefore draw transects perpendicular to the North Anatolian Fault system in the Sea of Marmara region and calculate line integrals for transform motion on them. For each realization from the Monte Carlo simulations, we compare the summed seismic slip implied by the earthquake rate model (coseismic slip/mean recurrence interval) and retain only those branches that fall within the entire observed geodetic rate of 23 ± 3 mm/yr, that is, the three strands of the North Anatolian Fault in the Marmara region [*Reilinger et al*., 2006; *Hergert et al*., 2011; *Ergintav et al*., 2014]. This slip rate must accommodate the sum of all rupture types on the same transect with their respective occurrence rate [see *Field and Page*, 2011, equation 1]. So they cannot be considered independently of each other, but their sum must fit the total slip rate. We assume complete seismic coupling in the absence of direct evidence for continuous fault creep throughout the seismogenic crust.

We consider a fully characteristic model with the recurrence time (T_r) being the basic ingredient to compute earthquake probability, both under a time-independent, Poissonian assumption and under a time-dependent, renewal approach. Since we do not have multiple characteristic events associated with the same fault segment, the value of T_r has to be derived by the combination of fault rupture parameters. We invoke conservation of seismic moment rate as proposed by *Field et al*. [1999]. The mean recurrence time in years (T_r) is computed as

$$T_r = \frac{\dot{M}_0}{\mu V A}, \tag{1}$$

where $\dot{M}_0 = 10^{(1.5M+9.05)}/t$ is the seismic moment rate of the fault segment, M is the magnitude, μ is the shear modulus ($\mu = 30$ GPa), V is the long-term slip rate in meters per year, defined as the ratio of shear stress to shear strain, and A is the fault area. The annual mean rate of characteristic earthquake occurrence is the inverse of the mean recurrence time. The coefficients 1.5 and 9.05 (SI units) in equation (1) are those proposed by *Hanks and Kanamori* [1979], *Anderson and Luco* [1983], and *WGCEP* [1995].

5.1. Moment-Balancing Multisegment Rupture Rates and Recurrence

We consider an alternative earthquake rupture model that includes the possibility that occasionally, more than one defined segment of the NNAF can connect up to generate higher-magnitude ruptures beneath the Sea of Marmara [e.g., *Le Pichon et al*., 2001, 2003]. Important issues are then how to define the proportion of ruptures that connect up relative to single-segment earthquakes and also to ensure that the overall fault zone moment budget is not violated.

We use a simple earthquake simulator [*Parsons and Geist*, 2009; *Parsons et al*., 2012] to calculate earthquake rupture rates on the NNAF as constrained by long-term average fault slip rate and GPS transects. We generate a cumulative slip budget over a sufficiently long model duration (100 kyr) for each segment that can join in multisegment ruptures (#1, 2, 4, 5, and 6 in Figure 1). There are 10 total combinations possible among these segments (1 + 2, 1 + 2 + 4, 1 + 2 + 4 + 5, 1 + 2 + 4 + 5 + 6, 2 + 4, 2 + 4 + 5, 2 + 4 + 5 + 6, 4 + 5, 4 + 5 + 6, and 5 + 6) with a magnitude range between $M_w = 7.0$ and $M_w = 8.0$ (calculated using the "Ellsworth B" relation [*WGCEP*, 2003]).

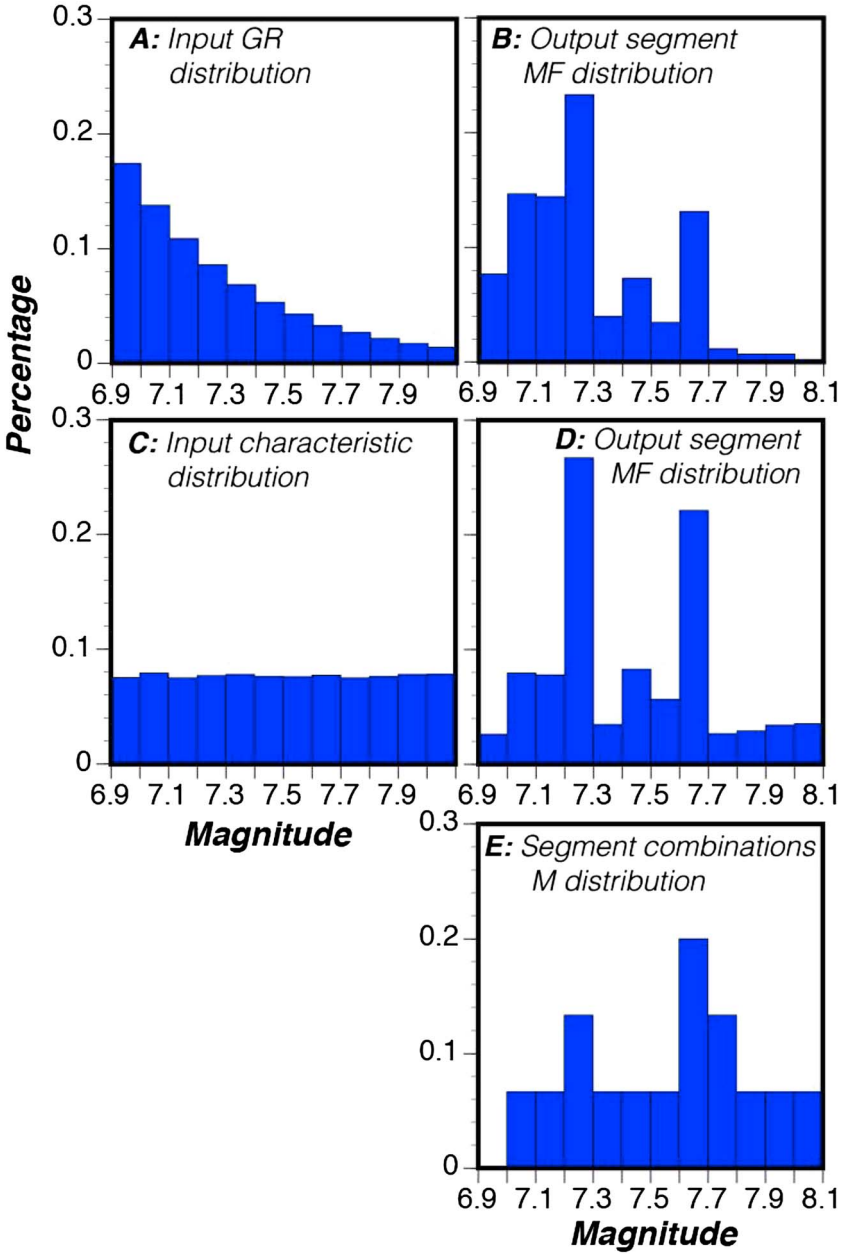

Figure 3. (a) The input magnitude-frequency (MF) distribution of trial ruptures and (b) the resulting distributions of ruptures that fit the segmentation and slip rates. (c and d) The same information is plotted except that the input distribution (Figure 3c) is characteristic. (e) The relative percentage of available magnitudes is shown, which is dependent on the segment definitions shown in Figure 1.

We populate the NNAF faults with earthquake ruptures until the slip budgets for each segment are used up. Trial earthquake magnitudes are drawn at random from a predefined magnitude-frequency distribution.

We use two different distributions, a power law *Gutenberg-Richter* (GR) distribution [*Gutenberg and Richter*, 1956] and a *characteristic distribution* (CH) to assess the effects of input magnitude-frequency distribution. A characteristic model departs from the log-linear relationship of a *Gutenberg-Richter* model by distributing a variable amount of the moment into larger-magnitude events. The exact proportion of this shift is not explicitly defined and can vary from fault to fault. We therefore begin with an input model with a uniform magnitude-frequency distribution (CH, $b = 0.0$) and a GR model ($b = 1.0$) and allow the fault geometry to define magnitude rates.

Table 3. Multisegment Rupture Recurrence Intervals Calculated as a Function of Defined Slip Rate Budgets for the NNAF[a]

Segments Involved	*M*	GR MRI (yr)	CH MRI (yr)
1	7.6	236	354
2	7.0	235	917
4	7.1	301	806
5	7.2	382	990
6	7.2	196	268
1 + 2	7.7	7494	5201
1 + 2 + 4	7.8	6612	3341
1 + 2 + 4 + 5	7.9	5615	2402
1 + 2 + 4 + 5 + 6	8.0	3997	1264
2 + 4	7.3	1800	2788
2 + 4 + 5	7.6	4361	3833
2 + 4 + 5 + 6	7.7	9033	5128
4 + 5	7.4	764	1051
4 + 5 + 6	7.6	4370	3399
5 + 6	7.5	1033	1224

[a]GR stands for an input *Gutenberg-Richter* magnitude-frequency distribution and CH stands for characteristic distribution.

The average slip ($\bar{S}$) associated with the trial earthquake is calculated through the moment-magnitude relation of *Hanks and Kanamori* [1979] assuming a shear modulus of $\mu = 30$ GPa as

$$\bar{S} = \frac{10^{(1.5M+9.05)}}{\mu A}, \quad (2)$$

where A is the rupture area and μ is defined as the ratio of shear stress to shear strain. If the potential magnitude cannot be fit into the available area and slip budget, it is passed over and a new magnitude is attempted. Since we assign initial rupture locations at random, we must make multiple simulations to reduce the influence of the starting rupture locations.

Figures 3a and 3c give the input magnitude-frequency under the two assumptions (GR and CH), respectively. The results of the calculations (Figures 3b and 3d) indicate the percentage of possible events versus magnitude that fit the segmentation and slip rates for GR and CH distributions, respectively. The limited magnitude options inherent to the segment definitions mean that the output rupture rates are not extremely sensitive to the input magnitude-frequency distributions (Figure 3) except where expected, with more balance given to high-magnitude events at the expense of smaller ruptures in the characteristic input. Figure 3e shows the relative percentage of available magnitudes for all segment combinations. In Table 3, we give the magnitudes and the mean recurrence intervals (MRI) of all the single-segment and multisegment ruptures as a function of GR and CH distributions, respectively. The rates of each segment are provided as the inverse of the MRI. These mean recurrence intervals are used for both the single ruptures (#1, 2, 4, 5, and 6) and their 10 combinations in the probability computation.

The recently ruptured Izmit segment (#1) has a very small elapsed time ratio (0.068) in our model, and we interpret this to mean that it may take at least a couple of centuries for stress to build up to a level where it can rupture again (Table 1). In fact, in our combination probability computations, those ruptures along the multisegments that accommodate the recent Izmit single rupture (1 + 2, 1 + 2 + 4, 1 + 2 + 4 + 5, and 1 + 2 + 4 + 5 + 6) have very low rupture rates with respect to those of single ruptures. The reason is that the multisegment ruptures need more time to be synchronized to rupture together and, as a consequence, their occurrence becomes very unlikely in the Marmara region. Moreover, for many of those large multisegment events, we cannot even be sure that they have occurred in the region within the period of recording seismicity by historical and instrumental methods. In other words, existing earthquake catalogs and paleoseismic databases are not long enough to provide a reliable estimate of long-term recurrence for those multisegment events that have MRIs of several thousand years (Table 3). To overcome these difficulties, we use earthquake simulation algorithms [*Parsons et al.*, 2012; *Console et al.*, 2014] constrained by long-term slip rate to produce long histories of simulated earthquake catalogs. We show the ratio between the number of possible events in each single-segment and multisegment rupture with respect to the total number of events for GR and CH input magnitude-frequency distributions in Figures 4a and 4b, respectively; we find that 80% and 68% of events occurred on single-segment ruptures for the GR and CH input distributions.

6. Earthquake Probability Models

We used three probability models to represent the recurrence time probability distribution for single-segment and multisegment earthquakes: (1) the time-independent Poisson model, (2) the time-dependent BPT model, and (3) an interaction model based on the BPT distribution that includes the permanent effect

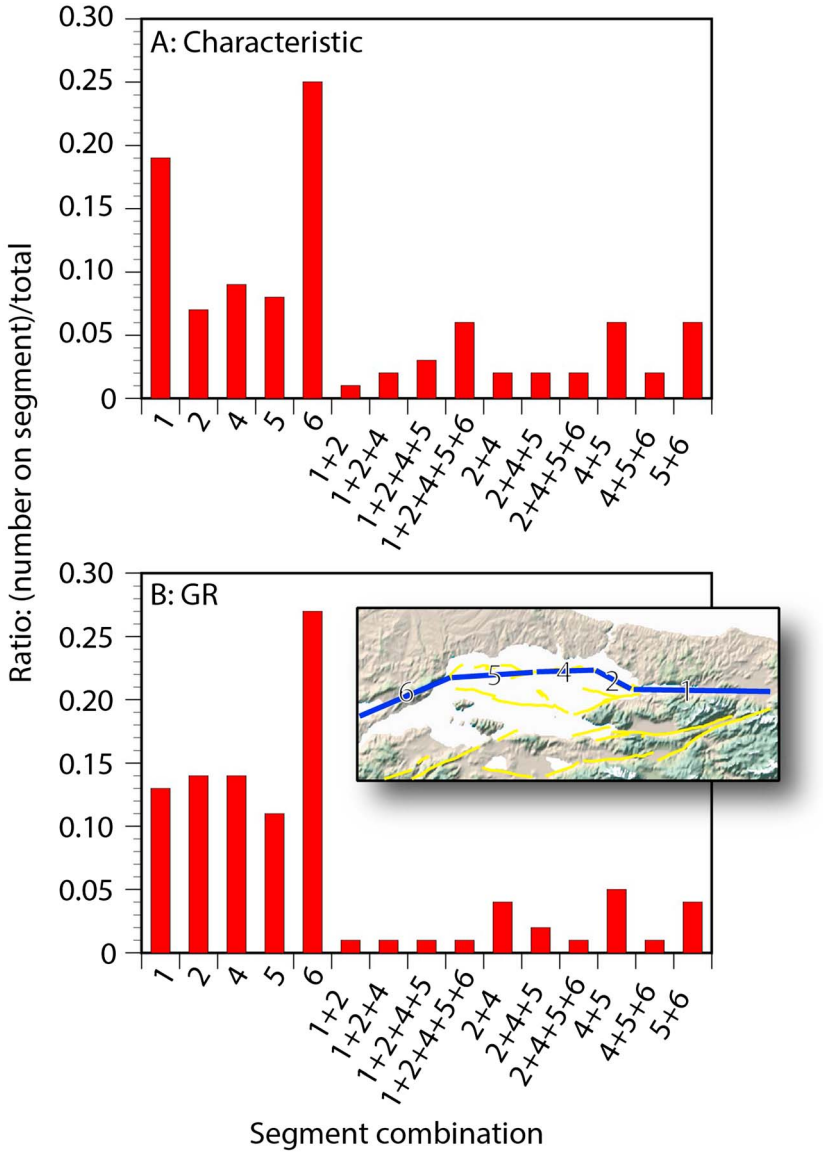

Figure 4. Proportion of the total number of possible multisegment earthquakes on each combination for (a) a characteristic input magnitude-frequency distribution and (b) and *Gutenberg-Richer* magnitude-frequency distribution. In these two examples, single-segment ruptures make up 68% of the total for the characteristic input and 80% for the *Gutenberg-Richter*. Numbers on the horizontal axes represent segment combinations as shown in Figure 1, and on the inset map.

of stress interaction among faults. For a uniform Poisson model, the expected recurrence time T_r is the only necessary parameter as

$$f(t) = \frac{1}{T_r}\exp\left\{-\frac{t}{T_r}\right\}, \tag{3}$$

where t is the interval of interest (exposure time).

In the BPT distribution, also known as the inverse Gaussian distribution [*Kagan and Knopoff*, 1987], the hazard function (the instantaneous value of the conditional rate density) begins at zero immediately after the last characteristic event and it increases continuously with elapsed time approaching to the recurrence time. It then is asymptotic to a constant level for elapsed times much larger than the average recurrence time. The probability density function [*Matthews et al.*, 2002] is given by

$$f(t;T_r,\alpha)=\left(\frac{T_r}{2\pi\alpha^2 t^3}\right)^{1/2}\exp\left\{-\frac{(t-T_r)^2}{2T_r\alpha^2 t}\right\}, \quad (4)$$

where t is the elapsed time from the last characteristic event and α is the coefficient of variation (also known as the aperiodicity) of the distribution.

The computation starts at the time of the last characteristic earthquake that occurred on each segment, and the elapsed time is reset to zero upon the occurrence of every subsequent characteristic event. The aperiodicity parameter describes how regularly or irregularly characteristic earthquakes are expected to occur on any fault. This parameter is ordinarily derived from the coefficient of variation of actual observed recurrence time intervals on individual faults and can be reinforced with geological evidence [*Ellsworth et al*., 1999; *Cramer et al*., 2000].

In the absence of any statistical assessment on aperiodicity due to the low number of events reported on each segment of the NAFZ, we have considered a range of aperiodicity values between 0.3 and 0.7 (0.5 ± 0.2).

It is well established that faults interact with one another through redistribution of stress caused by earthquakes, with a particularly clear example being the North Anatolian Fault [*Nalbant et al*., 1998; *Stein et al*., 1997]. We include these interactions by calculating Coulomb static stress change (ΔCFF) [*King et al*., 1994] as

$$\Delta\mathrm{CFF}=\Delta\tau+\gamma'\cdot\Delta\sigma_n, \quad (5)$$

where $\Delta\tau$ is the shear stress change in the slip direction on the receiving fault, $\Delta\sigma_n$ is the normal stress change acting on the receiver fault and γ' is the friction parameter, usually called the effective (or apparent) friction coefficient. It includes the effects of pore fluid as well as the material properties of the fault zone [see *Harris and Simpson*, 1998, for a deeper explanation of this parameter]. Values of γ' between 0 and 0.75 are considered plausible, with an average value of 0.4 that is widely used in studies of Coulomb stress modeling for major faults [e.g., *King et al*., 1994; *Harris and Simpson*, 1998; *Paradisopoulou et al*., 2010]. It is the value adopted in this study, which is an acceptable value as proposed by *Deng and Sykes* [1997a, 1997b] from the study of 10 years of seismicity in southern California. When γ' is high, it increases the tangential traction needed to break. At the other extreme, when $\gamma'=0$, the rock is so saturated that the pore pressure annihilates the effect of the normal stress on the plane [*Cattin et al*., 2009]. *Deng and Sykes* [1997a, 1997b] constructed a model of stress evolution in southern California for the period 1812–2025, highlighting that the stress patterns corresponding to the lowest γ' (0.2) are very similar to those obtained using a higher value (0.6). *Middleton and Copley* [2013] assemble a catalogue of well-constrained focal mechanisms for earthquakes that occurred on continental dip-slip faults and suggested, from the observed distributions, the reactivation of structures with a low coefficient of friction (less than ~0.3, and possibly as low as $\leq$0.1). They proposed that this low coefficient of friction corresponds to the presence of weak materials in preexisting fault zones.

For calculating the Coulomb failure function, knowledge of the fault parameters of the causative and receiving sources, as well as the focal mechanism (strike, dip, and rake), dimensions (width and length), and average slip for all the triggering earthquakes, is necessary. In our study, the cumulative stress change ΔCFF is computed by adding the contributions from all the other sources that have ruptured after the latest known earthquake on a given segment. The computation is carried out all over the source area for each node of a dense rectangular grid (2×2 km). The methodology adopted is described in detail by *Console et al*. [2013 and reference therein]. The algorithm for ΔCFF calculations assumes an Earth model with a half-space characterized by uniform elastic properties. Considering the absence of direct information about the slip distribution for the causative earthquakes, in this study, we have assumed for all of them a distribution consistent with a uniform stress drop (equal to 3.0 MPa) on the rectangle of the segment fault. We have calculated the slip distribution that satisfies the condition of zero slip on the edge and maximum at the center on the rectangle of the causative source [*Console and Catalli*, 2006].

The maximum value of the slip is defined through the relation

$$\Delta S_{\max}=\frac{16}{\pi^2}\frac{M_0}{\mu WL}, \quad (6)$$

where μ is the shear modulus of the elastic medium, W and L the dimensions of the causative fault (width and length, respectively), and M_0 is the seismic moment derived from the *Kanamori and Anderson* [1975] relation.

The effect of ΔCFF on the probability of future characteristic earthquakes assumes that the time elapsed since the previous earthquake is modified from t to t' by a shift, Δt, proportional to ΔCFF, that is,

Table 4a. Results of the Statistical Analysis Obtained for the 26 Single-Segment Ruptures Together With 10 Combinations of the Multiple-Segment Rupture Events, Considering the *Gutenberg-Richter* Frequency-Magnitude Distribution Model (GR) and a Conventional Date (10 September 1509) for Previous Rupture on Faults That Involve the Multiple-Segment Rupture Model to Calculate the Probability of Occurrences Beneath the Marmara Sea[a]

		Magnitude Source				Recurrence Time			Elapsed Time	Slip Rate (mm/yr)		
	Fault Name	16th Percentile	50th percentile	84th percentile	*T* elapsed up to 2015	16th Percentile	50th Percentile	84th Percentile	*Ratio T* elapsed/ (50th Percentile) Recurrence Time	16th percentile	50th percentile	84th percentile
1	Izmit	7.55	7.58	7.60	16	224	234	244	0.068	15.09	15.52	15.99
2	Çınarcık	6.99	7.02	7.04	121	224	240	257	0.504	7.45	7.98	8.52
3	South Çınarcık	7.14	7.17	7.19	52	390	452	530	0.115	4.25	5.04	5.86
4	Central Marmara	7.04	7.07	7.10	249	277	292	310	0.853	6.59	6.95	7.30
5	West Marmara	7.15	7.17	7.20	672	352	372	396	1.806	5.81	6.13	6.47
6	Ganos	7.23	7.26	7.29	103	192	202	212	0.510	11.99	12.51	13.04
MF001	Multiple Rupture #1#2	7.66	7.68	7.71	506	6897	7213	7515	0.099	0.55	0.57	0.59
MF002	Multiple Rupture #1#2#4	7.75	7.78	7.80	506	6065	6310	6575	0.153	0.71	0.73	0.75
MF003	Multiple Rupture #1#2#4#5	7.85	7.87	7.90	506	5475	5690	5928	0.214	0.88	0.90	0.92
MF004	Multiple Rupture #1#2#4#5#6	7.94	7.97	7.99	506	3776	3912	4061	0.408	1.43	1.45	1.48
MF005	Multiple Rupture #2#4	7.32	7.34	7.37	506	1670	1751	1843	0.188	1.52	1.59	1.65
MF006	Multiple Rupture #2#4#5	7.54	7.56	7.59	506	3890	4059	4240	0.132	0.86	0.88	0.91
MF007	Multiple Rupture #2#4#5#6	7.71	7.73	7.76	506	8158	8517	8835	0.103	0.50	0.51	0.53
MF008	Multiple Rupture #4#5	7.39	7.42	7.45	506	720	755	791	0.506	3.89	4.03	4.18
MF009	Multiple Rupture #4#5#6	7.62	7.64	7.67	506	4169	4337	4530	0.155	0.88	0.90	0.93
MF010	Multiple Rupture #5#6	7.49	7.52	7.54	506	1019	1063	1112	0.422	3.08	3.19	3.30
7	North Saros	7.11	7.14	7.17	103	197	216	238	0.477	9.30	10.20	11.10
8	South Saros	7.11	7.14	7.16	156	196	215	238	0.726	9.29	10.20	11.10
9	Mudurnu	7.20	7.22	7.25	48	220	242	267	0.198	9.10	10.00	10.90
10	Abant	7.09	7.12	7.14	58	199	217	240	0.267	9.02	9.90	10.80
11	Düzce	7.12	7.14	7.17	16	142	153	167	0.105	13.30	14.40	15.50
12	Gerede	7.10	7.13	7.15	71	84	88	91	0.811	24.30	24.70	25.20
13	Geyve	7.10	7.13	7.16	719	158	180	211	3.994	10.40	12.20	13.80
14	Iznik	7.11	7.14	7.16	596	162	191	225	3.120	9.74	11.60	13.30
15	Yenisehir	7.11	7.13	7.16	950	259	291	325	3.265	6.72	7.51	8.42
16	Gemlik	7.11	7.13	7.16	160	491	546	617	0.293	3.55	4.01	4.46
17	Bursa	7.10	7.13	7.16	872	276	322	387	2.712	5.63	6.78	7.87
18	South Marmara	7.10	7.13	7.16	459	637	738	872	0.622	2.50	2.96	3.43
19	Kemalpasa	7.11	7.13	7.16	160	216	249	297	0.644	7.36	8.78	10.10
20	Manyas	7.11	7.13	7.16	51	221	255	301	0.200	7.28	8.62	9.84
21	Bandirma	7.13	7.15	7.18	1892	644	741	893	2.553	2.51	3.01	3.46
22	Gönen	7.12	7.15	7.18	62	378	451	550	0.137	4.04	4.94	5.89
23	Biga	7.13	7.15	7.18	46	948	1170	1515	0.039	1.49	1.91	2.36
24	Pazarkoy	7.12	7.15	7.18	71	550	660	791	0.108	2.83	3.37	4.05
25	Can	7.12	7.15	7.18	278	646	746	874	0.373	2.54	2.98	3.46

AGU Journal of Geophysical Research: Solid Earth

10.1002/2015JB012595

Table 4a. (continued)

	Fault Name	Magnitude Source			Recurrence Time				Elapsed Time Ratio *T* elapsed/ (50th Percentile) Recurrence Time	Slip Rate (mm/yr)		
		16th Percentile	50th percentile	84th percentile	*T* elapsed up to 2015	16th Percentile	50th Percentile	84th Percentile		16th percentile	50th percentile	84th percentile
26	Ezine	7.12	7.15	7.18	343	907	1120	1500	0.306	1.50	2.00	2.46

[a]The values of the 16th, 50th, and 84th percentiles of the Monte Carlo procedure are given for the maximum magnitude, the recurrence time, the elapsed time, the elapsed time ratio, and the slip rates.

$$t' = t + \Delta t = t + \frac{\Delta \mathrm{CFF}}{\dot{\tau}}, \tag{7}$$

where the tectonic stressing rate ($\dot{\tau}$) is assumed unchanged by the stress perturbation, estimated from the segment slip rate (V) and the area of the earthquake source [*Console et al.*, 2008] as

$$\dot{\tau} = \frac{32\mu V}{\pi^2 \sqrt{A}}, \tag{8}$$

where V is the long-term slip rate in meters per year and A is the rupture area.

Usually, the Coulomb stress change ΔCFF varies over the surface of the target fault segment, often having negative and positive values. Positive values of ΔCFF promote the failure while the negative values suppress it and can cause a rupture delay. Recent studies found that a higher percentage of events occur in regions of stress increase rather than stress decrease [*Woessner et al.*, 2012; *Ishibe et al.*, 2015]. As we do not know where nucleation will take place, we take the average of the positive stress changes as an estimate of the stress increase that could prompt future earthquakes. Selecting the average of the positive region is reasonable even if we consider the stress condition before 1509, because from *Parsons* [2004] we have secular stressing rates from 0.001 to 0.0064 MPa/yr, which yields 0.5–3.2 MPa of stress accumulation since 1509 on the Marmara segments. This likely dwarfs any pre-1509 interaction effects.

We recalculate the 30 year probability starting from 1 January 2015 for the 26 considered faults of the Marmara region, and an additional 10 combinations of multisegment ruptures using clock changes (Δt, equation (7)) to modify last earthquake times. The BPT + ΔCFF model is thus conditioned by the elapsed time since the last characteristic earthquake on each fault, and by the history of subsequent earthquakes that occurred on neighboring segments [e.g., *Parsons*, 2004, 2005; *Console et al.*, 2008; *Falcone et al.*, 2010; *Console et al.*, 2013]. To determine the year of the last event on multisegment ruptures, we take into account two different hypotheses: (1) the last event of a multisegment rupture is the most recent event that occurred on any of its single segments or (2) the last multisegment rupture date is set as 10 September 1509 (M_s = 7.2–7.6), which is the oldest reliable historical earthquake (Table 1) and is one that may have crossed the Sea of Marmara [*Le Pichon et al.*, 2001, 2003]. For all other single segments of the Marmara region, we use the last event that occurred on these faults.

The input GR and CH distribution models have influence on the event rates of segments #1, 2, 4, 5, 6, and for their relative 10 combinations, and consequently the timing of occurrence of the various failure models. Additionally, the choice of the date of the last event on the multisegment ruptures influences the elapsed time in the BPT model. So we obtain the following four combinations: (1) GR model-1509 event, (2) CH model-1509 event, (3) GR model last event on any involved segment, and (4) CH last event on any involved segment. In the rest of this paper, we refer to the results obtained from the first two options (Tables 4a, 4b, 5a, and 5b). The other two are reported as supporting information.

7. Treatment of Parameter Uncertainties

We consider uncertainties in the mean recurrence interval, aperiodicity, maximum expected magnitude, slip rate, and consequently mean recurrence time (equations (1) and (2)) in our application of three probability models on 26 single and 10 multiple ruptured segments in the Marmara region. Magnitude

Table 4b. Results of the Statistical Analysis Obtained for the 26 Single-Segment Ruptures Together With 10 Combinations of the Multiple-Segment Rupture Events, Considering the *Gutenberg-Richter* Frequency-Magnitude Distribution Model (GR) and a Conventional Date (10 September 1509) for Previous Rupture on Faults That Involve the Multiple-Segment Rupture Model to Calculate the Probability of Occurrences Beneath the Marmara Sea[a]

		ΔCFF (MPa)			Poisson 30 Year Probability (%)			BPT 30 Year Probability (%)			BPT + ΔCFF 30 Year probability (%)		
#	Fault Name	16th Percentile	50th Percentile	84th Percentile	16th Percentile	50th Percentile	84th Percentile	16th Percentile	50th Percentile	84th percentile	16th percentile	50th percentile	84th percentile
1	Izmit	6.37E−01	6.86E−01	7.21E−01	11.6	12.0	12.5	0.0	0.0	0.2	0.1	0.6	2.1
2	Çınarcık	4.96E−01	5.37E−01	5.80E−01	11.0	11.8	12.5	10.3	13.3	15.8	13.3	15.5	17.7
3	South Çınarcık	9.21E−02	1.04E−01	1.12E−01	5.5	6.4	7.4	0.0	0.0	0.1	0.0	0.0	0.2
4	Central Marmara	1.89E−01	2.00E−01	2.12E−01	9.2	9.8	10.3	15.4	17.4	20.2	15.6	17.7	20.6
5	West Marmara	1.81E−01	1.95E−01	2.11E−01	7.3	7.8	8.2	13.4	16.6	21.6	13.4	16.6	21.7
6	Ganos	1.12E−01	1.19E−01	1.26E−01	13.2	13.8	14.4	13.1	16.3	18.3	14.0	16.9	18.9
MF001	Multiple Rupture #1#2	6.63E−02	7.14E−02	7.49E−02	0.40	0.42	0.43	0.00	0.00	0.00	0.00	0.00	0.00
MF002	Multiple Rupture #1#2#4	5.25E−02	5.64E−02	5.93E−02	0.46	0.47	0.49	0.00	0.00	0.02	0.00	0.00	0.03
MF003	Multiple Rupture #1#2#4#5	4.19E−02	4.49E−02	4.75E−02	0.51	0.53	0.55	0.00	0.04	0.17	0.01	0.07	0.24
MF004	Multiple Rupture #1#2#4#5#6	3.34E−02	3.59E−02	3.78E−02	0.74	0.76	0.79	0.77	1.46	2.11	1.04	1.73	2.34
MF005	Multiple Rupture #2#4	1.86E−01	2.13E−01	2.45E−01	1.61	1.70	1.78	0.00	0.01	0.08	0.02	0.13	0.37
MF006	Multiple Rupture #2#4#5	1.46E−01	1.57E−01	1.72E−01	0.71	0.74	0.77	0.00	0.00	0.00	0.00	0.00	0.03
MF007	Multiple Rupture #2#4#5#6	1.48E−0	1.56E−01	1.71E−01	0.34	0.35	0.37	0.00	0.00	0.00	0.00	0.00	0.00
MF008	Multiple Rupture #4#5	1.61E−01	1.69E−01	1.76E−01	3.72	3.90	4.08	2.11	2.98	3.59	3.91	4.34	4.79
MF009	Multiple Rupture #4#5#6	1.06E−01	1.14E−01	1.20E−01	0.66	0.69	0.72	0.00	0.00	0.02	0.00	0.01	0.06
MF010	Multiple Rupture #5#6	1.09E−01	1.19E−01	1.25E−01	2.66	2.78	2.90	0.90	1.67	2.31	1.88	2.54	3.04
7	North Saros	2.68E−03	2.93E−03	3.12E−03	11.8	13.0	14.1	9.6	13.8	17.4	9.6	13.8	17.4
8	South Saros	7.90E−01	8.82E−01	1.23E+00	11.9	13.0	14.2	17.6	20.9	24.4	19.5	23.0	27.0
9	Mudurnu	2.04E+00	2.18E+00	2.39E+00	10.6	11.7	12.7	0.2	1.3	3.6	10.2	13.2	15.5
10	Abant	7.75E−01	8.24E−01	1.13E+00	11.8	12.9	14.0	1.3	4.2	8.0	6.3	10.4	13.9
11	Düzce	0.00E+00	0.00E+00	0.00E+00	16.5	17.8	19.1	0.1	0.7	2.4	0.1	0.7	2.4
12	Gerede	3.38E−03	3.53E−03	3.71E−03	28.1	29.0	29.9	43.7	48.3	54.5	43.7	48.4	54.6
13	Geyve	8.07E−01	8.58E−01	9.19E−01	13.2	15.4	17.3	23.5	30.9	41.9	23.4	30.9	41.9
14	Iznik	5.02E−02	6.03E−02	6.73E−02	12.5	14.6	16.9	22.9	30.1	40.5	22.9	30.1	40.5
15	Yenisehir	5.81E−01	6.01E−01	6.47E−01	8.8	9.8	10.9	15.7	20.5	27.7	15.7	20.4	27.7
16	Gemlik	0.00E+00	0.00E+00	0.00E+00	4.8	5.4	5.9	0.3	1.3	2.9	0.3	1.3	2.9
17	Bursa	2.15E−01	2.26E−01	2.38E−01	7.5	8.9	10.3	14.2	18.9	26.3	14.2	18.9	26.3
18	South Marmara	1.86E−01	2.05E−01	2.14E−01	3.4	4.0	4.6	3.5	5.4	7.2	3.8	5.7	7.4
19	Kemalpasa	3.08E−01	3.39E−01	3.70E−01	9.6	11.4	13.0	11.5	16.6	21.3	12.8	17.6	22.2
20	Manyas	1.49E−02	1.58E−02	1.66E−02	9.5	11.1	12.7	0.1	1.0	3.5	0.2	1.1	3.6
21	Bandirma	3.86E−01	4.34E−01	4.79E−01	3.3	4.0	4.6	6.5	8.7	12.3	6.4	8.7	12.3
22	Gönen	2.03E−01	2.20E−01	2.32E−01	5.3	6.4	7.6	0.0	0.0	0.4	0.0	0.1	0.8
23	Biga	1.78E−03	2.04E−03	2.15E−03	2.0	2.5	3.1	0.0	0.0	0.0	0.0	0.0	0.0
24	Pazarkoy	0.00E+00	9.42E−04	1.48E−03	3.7	4.4	5.3	0.0	0.0	0.0	0.0	0.0	0.0
25	Can	3.17E−02	3.55E−02	3.92E−02	3.4	3.9	4.5	0.7	2.1	3.8	0.7	2.1	3.8

AGU Journal of Geophysical Research: Solid Earth

10.1002/2015JB012595

Table 4b. (continued)

#	Fault Name	ΔCFF (MPa)			Poisson 30 Year Probability (%)			BPT 30 Year Probability (%)			BPT + ΔCFF 30 Year probability (%)		
		16th Percentile	50th Percentile	84th Percentile	16th Percentile	50th Percentile	84th Percentile	16th Percentile	50th Percentile	84th percentile	16th percentile	50th percentile	84th percentile
26	Ezine	0.00E+00	0.00E+00	0.00E+00	2.0	2.6	3.3	0.1	0.6	1.9	0.1	0.6	1.9

[a]Occurrence probability on each considered fault segment of the next characteristic event, over 30 years starting on 1 January 2015, according to Poisson, BPT, and BPT + ΔCFF (the values refer to the average positive values of ΔCFF on each fault). The 16th, 50th, and 84th percentiles of the Monte Carlo distribution have been considered.

uncertainty of historical events affects the average dislocation of the slip at the fault center (equation (6)), which influences ΔCFF values. Recurrence times are calculated through equation (1) considering the uncertainties in the slip rate and magnitude. Variability in aperiodicity, maximum magnitude, and slip rate is represented by a Gaussian random variable truncated distribution at $\pm 2\sigma$ with mean equal to the estimated values. Aperiodicity, interevent time, and magnitudes are chosen by randomly drawing 1000 times in a Monte Carlo procedure. Then for each fault segment, the probability of occurrence for the window chosen (30 years starting from 1 January 2015) under Poisson, BPT, and BPT + ΔCFF models is computed, and the 16th, 50th, and 84th percentiles are identified. The 50th percentile represents the median of the probability distribution, while the 16th and 84th percentiles give the 68% confidence limits, ±1 standard deviation of the median. Therefore, the ranges given on calculated probabilities are defined in the same way with the percentile uncertainties for both the single-segment and multisegment ruptures using the GR model as well as the CH model distribution (Tables 4a, 4b, 5a, and 5b). From here on, the results are given as the 50th percentile values.

8. Results of the Analysis

8.1. Probability of Occurrence From Time-Independent (Poisson) Model

The results of the probabilities for the Marmara region under three models, shown in Table 4b, for the GR model-1509 event are plotted in a 2-D diagram (Figures 5a and 5b). Figure 5a shows the mean time-independent and time-dependent probability of occurrence from the GR earthquake model along with the 16th, 50th, and 84th percentiles of the corresponding simulated distribution for each single fault segment. As mentioned in section 6, the GR model is only applied for the #1, 2, 4, 5, and 6 segments and for their 10 multisegment combinations. For the other faults, the CH earthquake distribution is adopted. In Figure 5b, we show the probability results under three models for the 10 multisegment ruptures assumed beneath the Marmara Sea. As shown in Figures 5a and 5b, the mean occurrence probabilities under the Poisson model range from 0.35% (combination #2-4-5-6) to 29% (#12, Gerede fault). We note that the maximum values of the Poisson probability for the next 30 years are on those fault segments that have a high annual mean rate of earthquake occurrence (that is, the lowest values of recurrence time) and high slip rate. In the Poisson probability calculations, there are only uncertainties in the maximum expected magnitude and slip rate, and consequently the average recurrence time, which is derived from equation (1). In fact, considering the 50th percentile for the next 30 years, the largest value of the Poisson probability for single-segment ruptures is calculated east of the town of Bolu on the Gerede (#12) segment of the NAF, which last ruptured on 1 February 1944 and has an 88 year mean recurrence time based on a slip rate of 24.70 mm/yr (Tables 4a and 5a) [e.g., *Flerit et al*., 2003; *Meade et al*., 2002; *Reilinger et al*., 2006; *Straub et al*., 1997]. High values are also observed for the Geyve (13) and Düzce (#11) fault segments with Poisson probabilities of 15.4% and 17.8%, respectively (based on 180 and 153 year mean recurrence intervals). We calculated the Poisson probabilities for those fault segments that rupture individually (single-segment ruptures) for the different model assumptions (GR and CH) (given in Tables 4b and 5b).

For fault segments located beneath the Marmara Sea, we consider the possibility that secondary faults exist within step overs and that a rupture may go through segment boundaries, generating higher-magnitude ruptures.

Table 5a. Results of the Statistical Analysis Obtained for the 26 Single-Segment Ruptures Together With 10 Combinations of the Multiple-Segment Rupture Events, Considering the *Characteristic Earthquake Model* (CH) and a Conventional Date (10 September 1509) for Previous Rupture on Faults That Involve the Multiple-Segment Rupture Model to Calculate the Probability of Occurrences Beneath the Marmara Sea[a]

		Magnitude Source				Recurrence Time			Elapsed Time Ratio *T* elapsed/(50th Percentile) Recurrence Time	Slip Rate (mm/yr)		
	Fault Name	16th Percentile	50th percentile	84th percentile	*T* elapsed up to 2015	16th percentile	50th percentile	84th percentile		16th percentile	50th percentile	84th percentile
1	Izmit	7.55	7.58	7.60	16	341	356	371	0.068	9.94	10.22	10.53
2	Çınarcık	6.99	7.02	7.04	121	852	912	976	0.504	1.96	2.10	2.24
3	South Çınarcık	7.14	7.17	7.19	52	390	452	530	0.115	4.25	5.04	5.86
4	Central Marmara	7.04	7.07	7.10	249	770	813	864	0.853	2.37	2.49	2.62
5	West Marmara	7.15	7.17	7.20	672	921	973	1035	1.806	2.22	2.34	2.47
6	Ganos	7.23	7.26	7.29	103	267	281	294	0.510	8.64	9.02	9.40
MF001	Multiple Rupture #1#2	7.66	7.68	7.71	506	4857	5091	5312	0.099	0.78	0.81	0.84
MF002	Multiple Rupture #1#2#4	7.75	7.78	7.80	506	3168	3297	3438	0.153	1.35	1.39	1.43
MF003	Multiple Rupture #1#2#4#5	7.85	7.87	7.90	506	2271	2361	2460	0.214	2.11	2.17	2.22
MF004	Multiple Rupture #1#2#4#5#6	7.94	7.97	7.99	506	1196	1239	1286	0.408	4.50	4.59	4.69
MF005	Multiple Rupture #2#4	7.32	7.34	7.37	506	2563	2686	2829	0.188	0.99	1.04	1.08
MF006	Multiple Rupture #2#4#5	7.54	7.56	7.59	506	3691	3844	4026	0.132	0.90	0.93	0.96
MF007	Multiple Rupture #2#4#5#6	7.71	7.73	7.76	506	4700	4906	5089	0.103	0.87	0.89	0.91
MF008	Multiple Rupture #4#5	7.39	7.42	7.45	506	953	999	1046	0.506	2.94	3.05	3.16
MF009	Multiple Rupture #4#5#6	7.62	7.64	7.67	506	3129	3257	3402	0.155	1.17	1.21	1.24
MF010	Multiple Rupture #5#6	7.49	7.52	7.54	506	1151	1200	1255	0.422	2.73	2.83	2.92
7	North Saros	7.11	7.14	7.17	103	197	216	238	0.477	9.30	10.20	11.10
8	South Saros	7.11	7.14	7.16	156	196	215	238	0.726	9.29	10.20	11.10
9	Mudurnu	7.20	7.22	7.25	48	220	242	267	0.198	9.10	10.00	10.90
10	Abant	7.09	7.12	7.14	58	199	217	240	0.267	9.02	9.90	10.80
11	Düzce	7.12	7.14	7.17	16	142	153	167	0.105	13.30	14.40	15.50
12	Gerede	7.10	7.13	7.15	71	84	88	91	0.811	24.30	24.70	25.20
13	Geyve	7.10	7.13	7.16	719	158	180	211	3.994	10.40	12.20	13.80
14	Iznik	7.11	7.14	7.16	596	162	191	225	3.120	9.74	11.60	13.30
15	Yenisehir	7.11	7.13	7.16	950	259	291	325	3.265	6.72	7.51	8.42
16	Gemlik	7.11	7.13	7.16	160	491	546	617	0.293	3.55	4.01	4.46
17	Bursa	7.10	7.13	7.16	872	276	322	387	2.712	5.63	6.78	7.87
18	South Marmara	7.10	7.13	7.16	459	637	738	872	0.622	2.50	2.96	3.43
19	Kemalpasa	7.11	7.13	7.16	160	216	249	297	0.644	7.36	8.78	10.10
20	Manyas	7.11	7.13	7.16	51	221	255	301	0.200	7.28	8.62	9.84
21	Bandirma	7.13	7.15	7.18	1892	644	741	893	2.553	2.51	3.01	3.46
22	Gönen	7.12	7.15	7.18	62	378	451	550	0.137	4.04	4.94	5.89
23	Biga	7.13	7.15	7.18	46	948	1170	1515	0.039	1.49	1.91	2.36
24	Pazarkoy	7.12	7.15	7.18	71	550	660	791	0.108	2.83	3.37	4.05
25	Can	7.12	7.15	7.18	278	646	746	874	0.373	2.54	2.98	3.46

AGU Journal of Geophysical Research: Solid Earth

10.1002/2015JB012595

Table 5a. (continued)

	Fault Name	Magnitude Source			Recurrence Time			Elapsed Time Ratio	Slip Rate (mm/yr)		
		16th Percentile	50th percentile	84th percentile	*T* elapsed up to 2015	16th percentile	50th percentile	84th percentile	*T* elapsed/(50th Percentile) Recurrence Time	16th percentile	50th percentile	84th percentile
26	Ezine	7.12	7.15	7.18	343	907	1120	1500	0.306	1.50	2.00	2.46

[a]The values of the 16th, 50th, and 84th percentiles of the Monte Carlo procedure are given for the maximum magnitude, the recurrence time, the elapsed time, the elapsed time ratio, and the slip rates.

We attempt to determine the probability of multisegment ruptures for the five identified segments (1, 2, 4, 5, and 6) that can have 10 different combinations beneath the Marmara Sea (Tables 4a, 4b, 5a, and 5b). For the single-segment ruptures of the Marmara Sea faults, the largest Poisson probability is 14%, and 12–14 % for the Ganos (#6), Izmit (#1), and Çınarcık (#2) faults under the GR distribution model (Table 4b). The Ganos segment last ruptured on 9 August 1912 and has a modeled interevent time of 202 and 281 years according to GR and CH distributions, respectively. Similarly, the Izmit segment last ruptured on 17 August 1999, and its interevent time was calculated to be 234 and 356 years for the two different distribution models, yielding 30 year Poisson probabilities for this segment of 12% and 8%, respectively (Tables 5a and 5b). In general, the probability of occurrence is slightly lower under the characteristic earthquake model because more moment is devoted to higher magnitude, and thus less frequent earthquakes. As pointed out in section 5.1, the output rupture rates are not extremely sensitive to the input magnitude-frequency distributions (Figure 3) However, rupture probabilities for multisegment ruptures are much smaller compared to those of the single-segment events because recurrence rates decrease as a function of slip rate and rupture length. The largest Poisson probability is 3–4% with a *M*7.4 earthquake in the Marmara Sea region containing both the Central (#4) and West Marmara (#5) earthquake sources. The smallest occurrence probability of 0.5% is calculated for an *M*7.8 event and results from the Izmit and Çınarcık fault multisegment ruptures (#1 and #2) by a GR distribution (Figure 5b and Table 4b).

Additionally, a 30 year Poisson probability calculation is made for $M > \sim 7.0$ events as a combined model using the following equation:

$$P = 1 - (1 - P_n)(1 - P_{n-1})(1 - P_{n-2}) \cdots, \quad (9)$$

where n is the rupture number. Consequently, the combined Poisson probability of a $M > 7.3$ earthquake in the Marmara Sea is 51% for 2015–2045. It includes the aggregated probability of 10 multisegment ruptures together with the combined probability of single-segment ruptures, Izmit, Çınarcık, Central Marmara, Western Marmara, and Ganos earthquake sources (Figure 5b and Table 4b).

The aggregated probability is slightly lower (44%) when we assume only the combined probability of the six single-segment ruptures ($M > 7.0$). The contribution of the multiple rupture events to the combined probability in the region is relatively small compared with single-segment ruptures because the frequency of large-magnitude events ($M > 7.3$) is lower than that for smaller-magnitude events ($M > 7.0$).

The lowest values for the 50th percentile of the Poisson probability are found for the Ezine (#26) and Biga (#23) single fault segments, at about 2.5% (Tables 4b and 5b). The reason is due to their low slip rates (~2.0 mm/yr) and a magnitude computed of *M*7.2. These faults tend to have large recurrence intervals (1120 and 1170 years, respectively) and thus represent a low probability of occurrence (Tables 4a and 5a).

8.2. Probability of Occurrences From a Time-Dependent (BPT) Model

For calculating time-dependent probabilities of earthquake recurrence, one needs the mean recurrence time, the coefficient of variation, and the date of the most recent earthquake that resets the clock on the stress state of the fault back or forward to some initial value. The paleoseismological data in the Marmara region are sparse and apply to seismogenic sources along the onland part of the NNAF. Seismological data span only the last 110 years with

Table 5b. Results of the Statistical Analysis Obtained for the 26 Single-Segment Ruptures Together With 10 Combinations of the Multiple-Segment Rupture Events, Considering the *Characteristic Earthquake Model* (CH) and a Conventional Date (10 September 1509) for Previous Rupture on Faults That Involve the Multiple-Segment Rupture Model to Calculate the Probability of Occurrences Beneath the Marmara Sea[a]

		ΔCFF (MPa)			Poisson 30 Year Probability (%)			BPT 30 Year Probability (%)			BPT+ΔCFF 30 Year Probability (%)		
#	Fault Name	16th percentile	50th percentile	84th percentile	16th percentile	50th percentile	84th percentile	16th percentile	50th percentile	84th percentile	16th percentile	50th percentile	84th percentile
1	Izmit	6.37E−01	6.86E−01	7.21E−01	7.78	8.09	8.43	0.00	0.00	0.00	0.00	0.08	0.47
2	Çınarcık	4.96E−01	5.37E−01	5.80E−01	3.03	3.24	3.46	0.00	0.00	0.05	0.01	0.12	0.47
3	South Çınarcık	9.21E−02	1.04E−01	1.12E−01	5.5	6.4	7.4	0.0	0.0	0.1	0.0	0.0	0.2
4	Central Marmara	1.89E−01	2.00E−01	2.12E−01	3.41	3.62	3.82	0.23	0.94	1.93	0.40	1.28	2.34
5	West Marmara	1.81E−01	1.95E−01	2.11E−01	2.86	3.04	3.21	4.01	4.55	5.12	4.20	4.71	5.32
6	Ganos	1.12E−01	1.19E−01	1.26E−01	9.69	10.14	10.63	3.35	6.47	9.03	4.01	7.16	9.65
MF001	Multiple Rupture #1#2	6.63E−02	7.14E−02	7.49E−02	0.56	0.59	0.62	0.00	0.00	0.00	0.00	0.00	0.00
MF002	Multiple Rupture #1#2#4	5.25E−02	5.64E−02	5.93E−02	0.87	0.91	0.94	0.00	0.00	0.00	0.00	0.00	0.00
MF003	Multiple Rupture #1#2#4#5	4.19E−02	4.49E−02	4.75E−02	1.21	1.26	1.31	0.00	0.00	0.00	0.00	0.00	0.00
MF004	Multiple Rupture #1#2#4#5#6	3.34E−02	3.59E−02	3.78E−02	2.31	2.39	2.48	0.00	0.00	0.00	0.00	0.00	0.01
MF005	Multiple Rupture #2#4	1.86E−01	2.13E−01	2.45E−01	1.06	1.11	1.16	0.07	0.30	0.73	0.35	0.82	1.32
MF006	Multiple Rupture #2#4#5	1.46E−01	1.57E−01	1.72E−01	0.74	0.78	0.81	0.00	0.00	0.00	0.00	0.00	0.01
MF007	Multiple Rupture #2#4#5#6	1.48E−0	1.56E−01	1.71E−01	0.59	0.61	0.64	0.00	0.00	0.00	0.00	0.00	0.00
MF008	Multiple Rupture #4#5	1.61E−01	1.69E−01	1.76E−01	2.83	2.96	3.10	5.17	5.70	6.29	6.20	6.78	7.75
MF009	Multiple Rupture #4#5#6	1.06E−01	1.14E−01	1.20E−01	0.88	0.92	0.95	0.00	0.00	0.00	0.00	0.00	0.00
MF010	Multiple Rupture #5#6	1.09E−01	1.19E−01	1.25E−01	2.36	2.47	2.57	1.63	2.47	3.09	2.53	3.18	3.67
7	North Saros	2.68E−03	2.93E−03	3.12E−03	11.8	13.0	14.1	9.6	13.8	17.4	9.6	13.8	17.4
8	South Saros	7.90E−01	8.82E−01	1.23E+00	11.9	13.0	14.2	17.6	20.9	24.4	19.5	23.0	27.0
9	Mudurnu	2.04E+00	2.18E+00	2.39E+00	10.6	11.7	12.7	0.2	1.3	3.6	10.2	13.2	15.5
10	Abant	7.75E−01	8.24E−01	1.13E+00	11.8	12.9	14.0	1.3	4.2	8.0	6.3	10.4	13.9
11	Düzce	0.00E+00	0.00E+00	0.00E+00	16.5	17.8	19.1	0.1	0.7	2.4	0.1	0.7	2.4
12	Gerede	3.38E−03	3.53E−03	3.71E−03	28.1	29.0	29.9	43.7	48.3	54.5	43.7	48.4	54.6
13	Geyve	8.07E−01	8.58E−01	9.19E−01	13.2	15.4	17.3	23.5	30.9	41.9	23.4	30.9	41.9
14	Iznik	5.02E−02	6.03E−02	6.73E−02	12.5	14.6	16.9	22.9	30.1	40.5	22.9	30.1	40.5
15	Yenisehir	5.81E−01	6.01E−01	6.47E−01	8.8	9.8	10.9	15.7	20.5	27.7	15.7	20.4	27.7
16	Gemlik	0.00E+00	0.00E+00	0.00E+00	4.8	5.4	5.9	0.3	1.3	2.9	0.3	1.3	2.9
17	Bursa	2.15E−01	2.26E−01	2.38E−01	7.5	8.9	10.3	14.2	18.9	26.3	14.2	18.9	26.3
18	South Marmara	1.86E−01	2.05E−01	2.14E−01	3.4	4.0	4.6	3.5	5.4	7.2	3.8	5.7	7.4
19	Kemalpasa	3.08E−01	3.39E−01	3.70E−01	9.6	11.4	13.0	11.5	16.6	21.3	12.8	17.6	22.2
20	Manyas	1.49E−02	1.58E−02	1.66E−02	9.5	11.1	12.7	0.1	1.0	3.5	0.2	1.1	3.6
21	Bandirma	3.86E−01	4.34E−01	4.79E−01	3.3	4.0	4.6	6.5	8.7	12.3	6.4	8.7	12.3
22	Gönen	2.03E−01	2.20E−01	2.32E−01	5.3	6.4	7.6	0.0	0.0	0.4	0.0	0.1	0.8
23	Biga	1.78E−03	2.04E−03	2.15E−03	2.0	2.5	3.1	0.0	0.0	0.0	0.0	0.0	0.0
24	Pazarkoy	0.00E+00	9.42E−04	1.48E−03	3.7	4.4	5.3	0.0	0.0	0.0	0.0	0.0	0.0
25	Can	3.17E−02	3.55E−02	3.92E−02	3.4	3.9	4.5	0.7	2.1	3.8	0.7	2.1	3.8

AGU Journal of Geophysical Research: Solid Earth

10.1002/2015JB012595

Table 5b. (continued)

#	Fault Name	ΔCFF (MPa)			Poisson 30 Year Probability (%)			BPT 30 Year Probability (%)			BPT+ΔCFF 30 Year Probability (%)		
		16th percentile	50th percentile	84th percentile	16th percentile	50th percentile	84th percentile	16th percentile	50th percentile	84th percentile	16th percentile	50th percentile	84th percentile
26	Ezine	0.00E+00	0.00E+00	0.00E+00	2.0	2.6	3.3	0.1	0.6	1.9	0.1	0.6	1.9

[a]Occurrence probability on each considered fault segment of the next characteristic event, over 30 years starting on 1 January 2015, according to Poisson, BPT, and BPT + ΔCFF (the values refer to the average positive values of ΔCFF on each fault). The 16th, 50th, and 84th percentiles of the Monte Carlo distribution have been considered.

limited spatial resolution until 1999 (Kandilli Observatory and Earthquake Research Institute: http://www.koeri.boun.edu.tr/sismo/indexeng.htm).

Since we do not have observational data of repeated earthquakes on the individual faults, we have used coefficient of variation values that are similar to those used by the RELM of the Southern California Earthquake Center [*SCEC*, 1994]. These reports described the recurrence density function using a lognormal distribution of recurrence times with aperiodicity that ranges between 0.3 and 0.7.

In Tables 4a and 5a, we present the elapsed time ratios for each source given as the ratio of the elapsed time from the last event divided by the mean earthquake recurrence interval, referred to as the average percentile between the 16th and 84th of the Monte Carlo distribution with its standard deviation for the GR and CH models, respectively. The probability values reported in Table 5b for multisegment ruptures are the same as in Table 4b because, for all the sources, we use a CH distribution except for segments 1, 2, 4, 5, and 6 and their combinations.

When we consider the 50th percentile for the next 30 years, the largest time-dependent probability values are found for the Gerede (#12), Geyve (#13), and Iznik (#14) segments in the eastern and southeastern parts of the Marmara region, near the cities of Bolu and Bursa (Figure 1 and Table 1). The highest time-dependent probability value is calculated for the Gerede segment (48.3%). Such probability is due to the elapsed time (71 years), by its last characteristic event (1944), very close to its recurrence time of 88 years (Table 4a). The Geyve (#13) and Iznik (#14) segments have BPT probabilities equal to 30.9% and 30.1%, respectively (Table 4b). The Geyve segment shows a long time lapsed (719 years) that is well beyond the average recurrence time (180 years). Similarly, the Iznik fault segment last ruptured on 15 March 1419, such that the elapsed time of 596 years is three times larger than its calculated interevent time of 191 years. The corresponding Poisson probabilities for the Gerede and Geyve segments are relatively small at 29.0% and 15.40%, respectively (Figure 5a). The BPT probability is larger than the Poisson probability when the elapsed time is close to, or exceeds, the interevent time. The BPT probabilities for recently ruptured segments such as the Izmit (#1) and Düzce (#11) faults are lower (0.0% and 0.7%, respectively) than the Poisson values (12.0 % and 17.8%) due to the short elapsed time (16 years) after the occurrence of their last events (17 August 1999 and 12 November 1999, respectively). The lowest BPT probabilities (0.0%) are also observed for the Gönen (#22), Biga (#23), and Pazarkoy (#24) faults, in the southwestern part of the Marmara Sea, because of low elapsed time ratios of 0.14, 0.04, and 0.11, respectively (Tables 4a and 4b). These results are due to recent events on these segments (March 1953, March 1969, and October 1944).

Beneath the Marmara Sea, the Central Marmara (#4), West Marmara (#5), and Ganos (#6) single-segment ruptures yield the highest time-dependent probabilities at 17.4%, 16.6%, and 16.3% for the GR model (Table 4b) compared to those calculated under the CH model assumption (0.94%, 5.55%, and 6.47% for #4, #5, and #6 fault segments, respectively). Of the identified fault segments capable of generating $M > 7.0$ earthquakes, the 50th percentile time-dependent probability is calculated to be significantly higher (two times larger) than the Poisson value only on the Central (#4) and West (#5) Marmara Faults. The combined time-dependent probability that includes #1, #2, and #4 single-segment and multisegment rupture events is 28% and 32%, respectively. If we include the West Marmara fault (#5), the combined probability of segments 1, 2, 4, and 5 is 40%, and the relative probability of combined multisegments becomes 44%. The values obtained under a Poisson hypothesis are similar (35%) to those obtained by the combined probability of these single-segment and multisegment ruptures (43%) (Figure 5b).

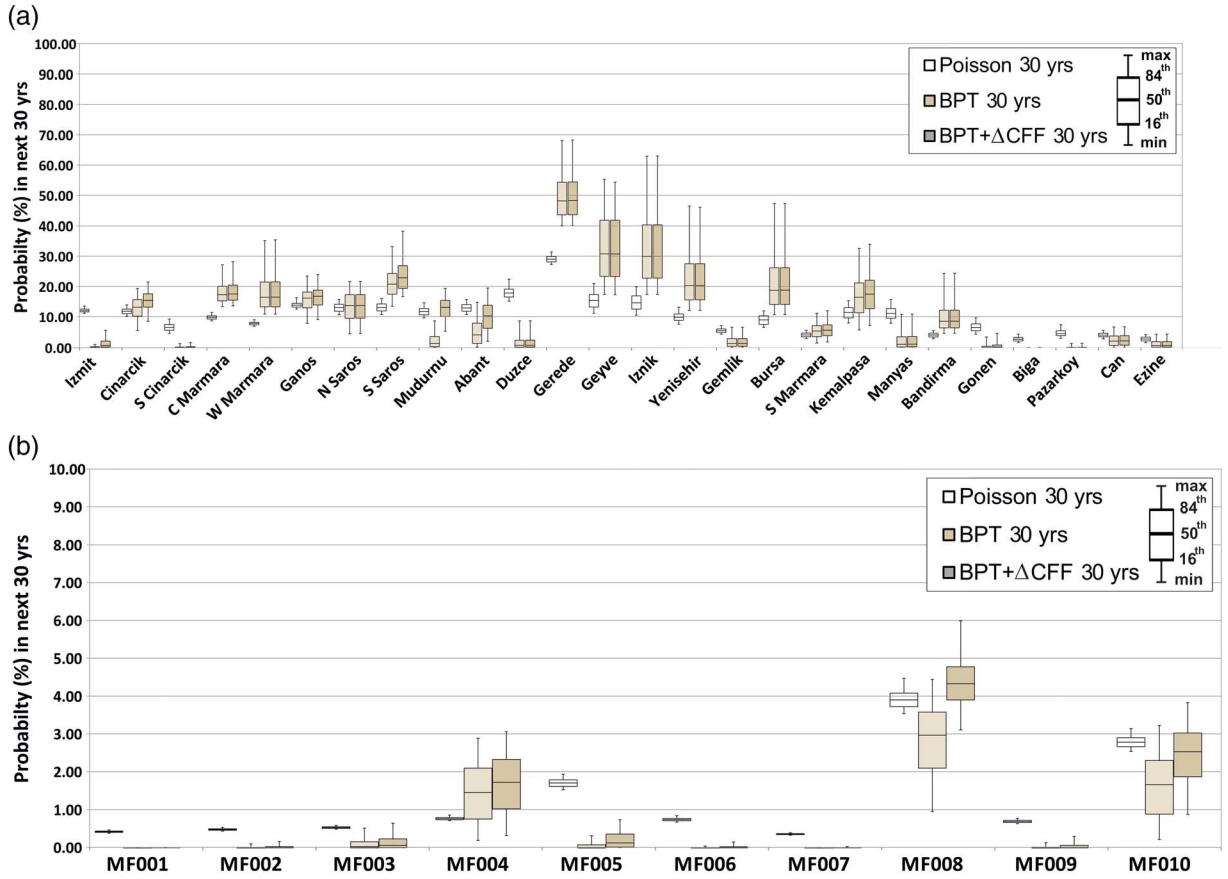

Figure 5. (a) Occurrence probabilities from a *Gutenberg-Richter* magnitude-frequency distribution model for each single-segment rupture event over 30 years starting on 1 January 2015 according to Poisson, BPT, and BPT + ΔCFF. For each model, the probability values related to the 16th, 50th, and 84th percentiles are shown in the plot. The elapsed time from the last characteristic event is computed from the 10 September 1509 event for each multiple ruptures. The strings on the abscissa refer to the 10 multiple breaks as referred in Tables 4a and 4b. (b) Occurrence probabilities from a *Gutenberg-Richter* magnitude-frequency distribution model for multiple-segment rupture events over 30 years starting on 1 January 2015 according to Poisson, BPT, and BPT + ΔCFF. For each model, the probability values related to the 16th, 50th, and 84th percentiles are shown in the plot. The elapsed time from the last characteristic event is computed from the 10 September 1509 event for each multiple ruptures. The strings on the abscissa refer to the 10 multiple breaks as referred in Tables 4a and 4b.

The time-dependent probability values we report are based on an elapsed time (506 years) calculated from the 10 September 1509 event as the last earthquake time on faults that involve the multiple-segment rupture model. We also examined the probability of occurrences for the multiple-segment ruptures using the most recent earthquake that occurred on any of the 10 combinations of fault segments. Due to some relatively short elapsed times since the last earthquakes compared to their mean recurrence time, we obtain smaller time-dependent probabilities using that assumption. These results can be found as supporting information in the manuscript (Tables S3, S4, S5, and S6).

The 30 year probability for large earthquakes affecting Istanbul can be considered to be around 28–32% based on the closest faults to this highly populated city. The combined Poisson probability (30–36%) is slightly larger than the time-dependent probability for Istanbul because of the recency of the 1999 Izmit earthquake on segment #1.

8.3. Time-Dependent Model With the Inclusion of Coulomb Stress Change

The time-dependent seismic earthquake occurrence rate obtained by the BPT distribution on each fault is successively modified by the inclusion of a permanent physical effect due to the Coulomb static stress change caused by failure of neighboring faults since the latest characteristic earthquake on the fault of interest. As pointed out by *Hubert-Ferrari et al.* [2002], small stress increases (~0.5 MPa) are sufficient to trigger failure in the upper crust. Similar observations are obtained using a Coulomb stress interaction approach in Western Turkey by *Paradisopoulou et al.* [2010].

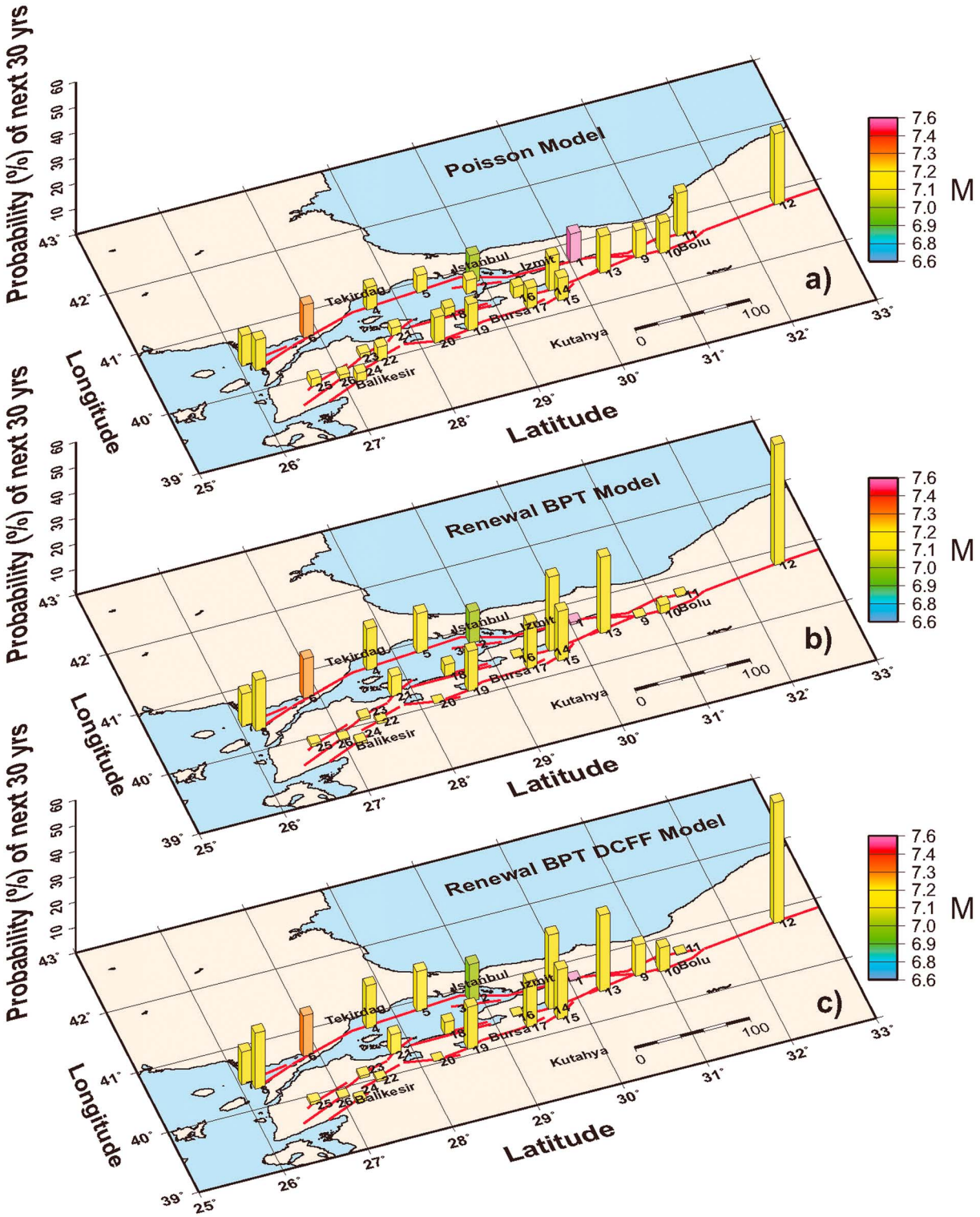

Figure 6. Probability of occurrence of the next characteristic earthquake over 30 years for the fault segments of the Marmara region computed starting on 1 January 2015, according to (a) Poisson, (b) BPT, and (c) BPT + ΔCFF models. The height of the bars corresponds to the 50th percentile probability of occurrence; colors correspond to the magnitude of each segment; the red line presents the fault surface rupture.

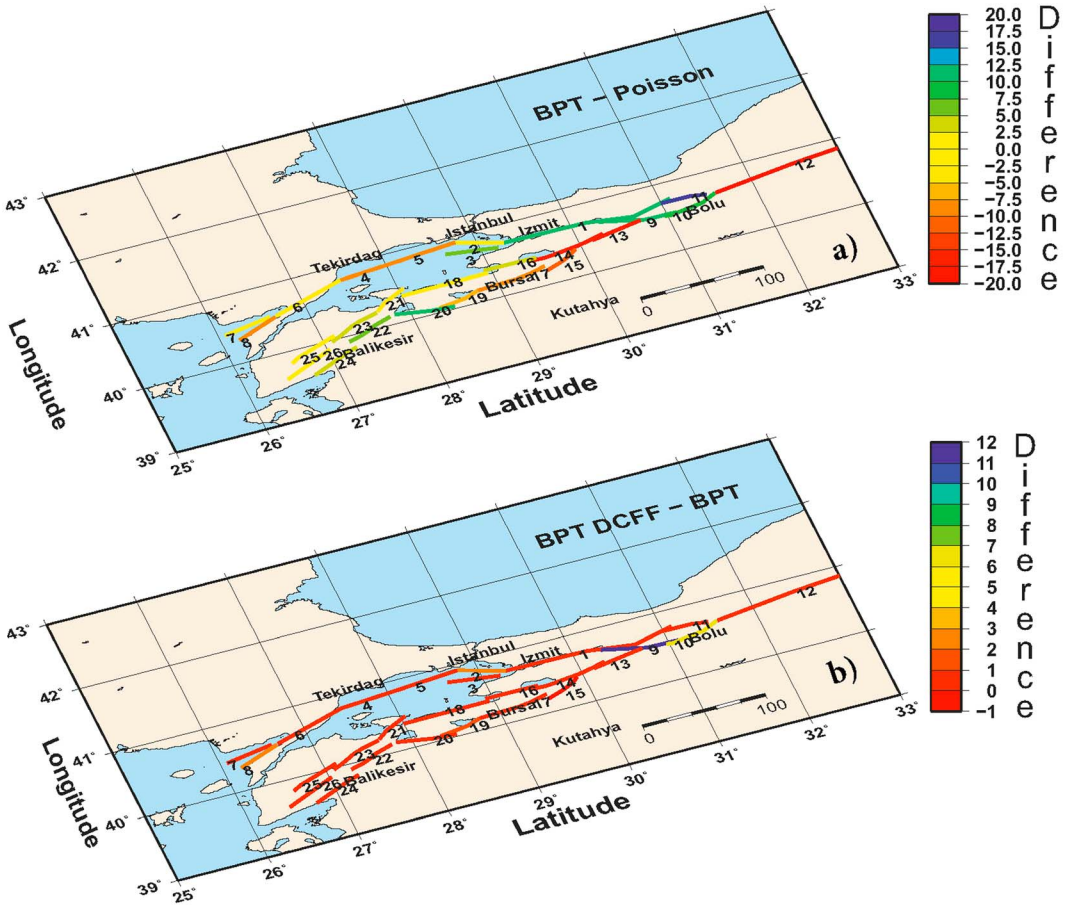

Figure 7. The difference in the occurrence probability of the next characteristic earthquake over 30 years for the examined region computed starting on 1 January 2015, between (a) BPT and Poisson models and (b) BPT + ΔCFF and BPT models, respectively.

Interaction probabilities are given in Table 4b for three models adopted and are shown in Figures 6a, 6b, and 6c for the 50th percentile probability of occurrence. The difference in probability between BPT and Poisson and BPT + ΔCFF and BPT models, respectively, are shown in Figures 7a and 7b. The results in Tables 4b and 5b show a small Coulomb stress change influence on probability when the faults close to the source under consideration produced the last event after its latest characteristic earthquake. Small effects are also obtained when the last earthquake on the neighboring faults has occurred later, but it was located at a distance (or had a focal mechanism) that did not produce a significant change in the ΔCFF. Considering the 50th percentiles of the Monte Carlo distribution, we observe that the highest positive stress interaction is for the Mudurnu (#9) fault, because the most recent earthquake occurred on 22 July 1967. The Mudurnu fault segment is located near the southern part of the Düzce fault segment, and very close to the recently ruptured Izmit fault (Figure 1). This fault was mostly affected by the transfer of stress from the Düzce earthquake of 12 November 1999. The static stress is raised by 2.18 MPa. The 1999 Izmit event increased the stress beyond the east end of the rupture by 0.1–0.2 MPa where the Düzce earthquake struck and by 0.05–0.5 MPa beyond the west end of the 17 August rupture where a cluster of aftershocks occurred [*Parsons et al.*, 2000; *Parsons*, 2004]. A lower value of ΔCFF (~1.2 MPa) for the Mudurnu fault was found by *Utkucu et al.* [2003], using a coseismic slip distribution model calculated using finite-fault inversion of teleseismic *P* and *SH* waveforms of the 12 November 1999 Düzce earthquake.

In our model, the high value (2.18 MPa) obtained for the Mudurnu segment (#9) could be related to the proximity to the Izmit fault (#1) and the small difference in strike between two faults, 85° and 84°, respectively, apart from the different slip distribution applied in the model. Another reason could be the size of the grid (2 × 2 km) chosen in our analysis. For the South Saros (#8) and Abant segments (#10) located in the western and eastern

parts of the Marmara region, the stress interaction is positive. In fact, both faults present a ΔCFF of 0.8 MPa. For the South Saros fault segment, the 50th percentile of the Monte Carlo distribution gives in the next 30 years a 20.9% and 23.0% of probability of occurrence, for the BPT renewal and BPT + ΔCFF models, respectively (Figure 5a and Table 4b). This fault is mostly affected by the Ganos (*M*7.3) and North Saros (*M*7.1) earthquakes that occurred on 9 August and 13 September 1912, respectively. The Abant fault segment (#10) is almost parallel to the Düzce fault (#11) and is affected by the 1999 event. The probability of occurrence increases up to 10.4% compared with standard renewal value of 4.2%.

The Izmit fault (#1) shows a stress change of 0.6 MPa due to the transfer of the stress caused by the occurrence of the event of 12 November 1999 on the Düzce fault segment (#11). However, both the BPT and BPT + ΔCFF model probability values are still small (0.0% and 0.6%, respectively) for the next 30 years after 1 January 2015. The stress change for the Düzce fault (#11) is equal to zero because the latest known earthquake on the fault is also the last earthquake in the catalog and no other large event on the neighboring faults has occurred since 12 November 1999. Considering the next 30 years, the 50th percentile probability for this fault from the BPT + Δ*CFF* model is the same as the probability from the simple renewal BPT model that is equal to 0.7%.

Examining the rupture probability beneath the Marmara Sea and around Istanbul for the next 30 years, we observe a maximum positive stress change of 0.54 MPa on the Çınarcık fault segment (#2), which is mostly affected by the 1999 Izmit earthquake. This positive stress change increases the probability of occurrence from 13.3% to 15.5% considering the BPT and BPT + ΔCFF, respectively. For the rest of the Marmara Sea faults, the positive stress change is lower (~0.2 MPa) as the influence of the Izmit earthquake diminishes toward the west. Again, the probability of occurrence is lower for the characteristic earthquake model (Table 5b). For example, for the Ganos fault segment (#6), the probability under the BPT + ΔCFF model is ~16.9% from the GR model (Table 4b) compared to 7.16% from the CH model (Table 5b). The combined probability of $M > 7.0$ earthquakes around Istanbul considering the single segments (#1, 2, 4, and 5), and incorporating both time dependence and stress transfer into the calculations, is 42%. It increases up to 47% considering both single- and multiple-segment ruptures (Figure 5b).

9. Discussion and Conclusions

We have applied in the Marmara region three earthquake occurrence models (Poisson, BPT, and BPT + ΔCFF) to an upgraded fault segmentation model based on new knowledge of the North Anatolian Fault Zone (NAFZ) configuration, for examining their effect on characteristic earthquake rupture forecasts for the next 30 years, starting on 1 January 2015. Moreover, since the Main Marmara fault could rupture in a great earthquake by linking up the individual segments across the Marmara Sea, the probability to have a strong event at Istanbul for the time period 2015–2045 has been also reviewed under this hypothesis.

In this study, the epistemic uncertainties are explored for the earthquake rupture forecast. The consideration of such uncertainties is important both to quantify the range of values for a given rupture probability and also to illustrate which model assumptions lead to the most significant variation in the calculated values.

The overall uncertainties on the source parameters (α, T_r, and M) together with their related parameters are included into the probability calculations simultaneously through a Monte Carlo approach. Uncertainty on each parameter is represented by the 16th, 50th and 84th percentiles of the simulated values. The choice of fault parameters influences the results of the earthquake rate forecasting models. The geometrical parameters of the fault together with the expected magnitude and long-term slip rate have an influence on the computation of the mean recurrence time, which is the basic ingredient to compute earthquake probability, both under a time-independent Poisson assumption and in time-dependent renewal approaches. The results of the present study clearly illustrate the influence of fault parameters on the probability calculations. As can be seen in Figures 5a and 5b, the dispersion around the 50th percentile time-dependent probabilities (given by the 16th and 84th percentiles) is mostly asymmetric because the distributions of the probability density functions that are estimated from the Monte Carlo approach take a mostly lognormal distribution form for each fault segment. The occurrence probability is nearly doubled with respect to its median value for those faults that have large elapsed time ratios (i.e., Geyve, Iznik, and Bursa), while it decreases only 0.5 times with respect to its median (Figures 5a and 5b).

In some cases, we have recurrence times T_r smaller than the elapsed time since the last earthquake. These values have a major influence on the probability from the renewal models. In fact, for the Geyve (#13),

Iznik (#14), Yenisehir (#15), Bursa (#17), and Bandirma (#21) faults, the elapsed time ratio is larger than 2.5, meaning that the elapsed time is more than twice the mean recurrence time. Therefore, they present larger probability of occurrence in the next 30 years (Figures 5a, 6b, and 6c). We also obtain larger probability values for faults like the Gerede (#12), South Saros (#8), and Central Marmara (#4) faults, which have an elapsed time ratio close to 1 (0.7–0.8). Moreover, the effect of the α parameter uncertainty is reflected in the probability calculation through the Monte Carlo simulations. In other words, considering a renewal model increases the overall uncertainty in occurrence probability compared to the uncertainty over the Poisson model, as there are more parameters involved.

The behavior of a BPT model depends strongly on the value of α, so that its hazard function increases with decreasing values of α and becomes Poisson-like with values that approach 1.0. This effect gets more pronounced depending on the proximity in time of the latest event on the fault that dominates the probability value at a given site. From the uncertainties (16th and 84th percentiles) presented in Figures 5a and 5b, it is difficult to follow the details of the behavior of each fault as a function of elapsed time, and the parameters that most influence the uncertainty in the probability estimates and/or contribution of each of those parameters to the overall uncertainty.

The interaction model of BPT + ΔCFF feels the effect of both the dimensions and the mechanism of the fault. The Coulomb static stress change is affected by all these parameters, while the tectonic stressing rate that varies the clock change depends on fault geometry. We calculated a strong increase in the probability of occurrence for the next 30 years on the Mudurnu (#9) fault segment considering the BPT + ΔCFF model, which was caused by the positive stress transfer accumulated from the 12 November 1999 Düzce earthquake. The interaction probability of occurrence is increased almost 10 times compared with the simple renewal model (1.3% versus 13.8%) because of a 2.18 MPa stress increase. For the rest of the Marmara region faults, we did not observe any significant variation of the probability obtained from the renewal models with the introduction of stress transfer.

The probability to have a strong event at Istanbul comes mainly from the Central (#4), Western Marmara (#5), and Çınarcık (#2) fault segments. The time-dependent probabilities under the BPT model are 17.4%, 16.6%, and 13.3%, for each single-segment rupture. Taking into account the stress change effect, these probabilities are modified slightly to 17.7%, 16.6%, and 15.4%, respectively. The combined Poisson probability that at least one of these three faults will rupture in the next 30 years is 26.6%. Considering the time-dependent model together with the stress interaction, the combined probability increases up to 42% if multisegment ruptures are allowed. These findings are in agreement with those of *Parsons* [2004] who found that the probability of having an earthquake ($M \geq 7.0$) close to Istanbul rises from a Poisson estimate of 21% to values of 41% under the time-dependent interaction model and are also similar to calculations by *Bohnhoff et al.* [2013] and *Paradisopoulou et al.* [2010]. Considering the stress transfer effect from the Izmit earthquake in the calculations, the combined probability to have an event with $M \geq 7.0$ up to $M8.0$ at Istanbul city, obtained by the BPT + ΔCFF model with the contribution of #1, 2, 4, and 5 single faults and their multisegment combinations, becomes 47%.

In this study, we incorporate uncertainties for fault source parameters (fault length, fault width, and slip rates) and their resulting recurrence rates in the calculation of probability of occurrence without going further to assess the relative contribution of each fault to the seismic hazard, as would be done in PSHA. However, our results as well as the parameters obtained in the present study are crucial, and the primary components in establishing the probabilistic seismic hazard map that is used for risk mitigation in many countries, being the foundation of the building code definition.

We would like to note that our fault model is based on an assumption of complete fault coupling and thus ignores the probability of aseismic creep on any of the fault segments. Neglecting the possibility of aseismic creep may lead to a bias toward higher seismic hazard according to the UCERF2 and UCERF3 models [*Field et al.*, 2014] where the seismic moment rates are reduced due to observed creeping processes on some California faults [*Weldon et al.*, 2013]. Slip rate reductions on highly creeping faults act to limit the rate of throughgoing ruptures [*Page et al.*, 2013]. Recently *Noda and Lapusta* [2013] presented a "plausible physical mechanism" for ruptures passing completely through the creeping section of the San Andreas Fault. They suggested that currently creeping fault regions, which are thought to be stable and aseismic, may participate in destructive events and host large seismic slip. Although the North Anatolian Fault (NAF) system is one of the best studied fault systems in Turkey, the fault characteristics and parameters which are crucial for a complete

moment-balanced PSHA still involve large uncertainties (see Table 1). Furthermore, the existing seismic observations lack the spatial and temporal resolution required to accurately distinguish differences between locked and creeping segments in the NAFZ. At present, we do not have enough reliable information on the creep rate, especially for those segments located in the Marmara Sea, close to the city of Istanbul. An exception is the Ismetpasa segment, within the 1944 earthquake rupture area that is located in the eastern part of the Marmara region. *Cakir et al*. [2005] estimated a 8 ± 3 mm/yr creeping rate, and the spatial extent of the Ismetpasa creeping segment using interferometric synthetic aperture radar data (from 1992 through 2001) suggesting also that the NAF at Ismetpasa does not creep at seismogenic depth, unlike the creeping segment of SAF on the north of Parkfield [*Özakın et al*., 2012; *Kaneko et al*., 2013]. Recently, *Bohnhoff et al*. [2013] identified a 30 km long fault patch that is entirely aseismic down to a depth of 10 km and locked. They suggested a scenario for the NAFZ segments of the Marmara Sea that is similar to that of the 2010 M_w8.8 Maule Chile event, which nucleated in a region of high locking gradient and ended up releasing most of the stress accumulated along the fault since the last major event. In fact, our fault model in the present paper considers a multisegment rupture model that allows higher-magnitude ruptures over some segments of the northern branch of the North Anatolian Fault Zone (NNAF) beneath the Marmara Sea.

Here we highlighted those sources in which time dependence may produce a significant increase or decrease in ground shaking hazard [*Akinci et al*., 2009] in the Marmara region. Further studies may be used to understand the impact of earthquake recurrence models on the PSHA estimate. These issues are worthy of further investigation in the next step.

Acknowledgments

This work has been partially supported by the MARSite (Marmara Supersite) "New Directions in Seismic Hazard Assessment through Focused Earth Observation in the Marmara Supersite," European Integrated Project, THEME-ENV.2012.6.4-2 (Long-term monitoring experiment in geologically active regions of Europe prone to natural hazards: the Supersite concept), grant agreement 308417. Authors are grateful to David Rhoades, Eleftheria Papadimitriou, and Vassilis Karakostas for the useful discussions and suggestions also on the statistical treatment of data. In this paper, some figures were prepared using the Generic Mapping Tools version 4.2.1. All data and software are freely available from the authors.

References

Akinci, A., F. Galadini, D. Pantosti, M. Petersen, L. Malagnini, and D. Perkins (2009), Effect of time dependence on probabilistic seismic-hazard maps and deaggregation for the central Apennines, Italy, *Bull. Seismol. Soc. Am.*, *99*, 585–610.

Akinci, A., D. Perkins, A. M. Lombardi, and R. Basili (2010), Uncertainties in the estimation of the probability of occurrence of strong earthquakes from individual seismological sources in the Apennines, Italy, *J. Seismol.*, *14*, 95–117.

Aksoy, M. E., M. Meghraoui, M. Vallée, and Ç. Ziyadin (2010), Rupture characteristics of the A.D. 1912 Mürefte (Ganos) earthquake, segment of the North Anatolian fault (western Turkey), *Geology*, *38*(11), 991–994, doi:10.1130/G31447.1.

Aksu, A. E., T. J. Calon, R. N. Hiscott, and D. Yasar (2000), Anatomy of the North Anatolian fault zone in the Marmara sea, western Turkey: Extensional basins above a continental transform, *GSA Today*, *6*, 3–7.

Altunel, E., M. Meghraoui, H. S. Akyuz, and A. Dikbas (2004), Characteristics of the 1912 coseismic rupture along the North Anatolian Fault Zone (Turkey): Implications for the expected Marmara earthquake, *Terra Nova*, *16*(4), 198–204.

Ambraseys, N. (1970), Some characteristic features of the Anatolian fault zone, *Tectonophysics*, *9*, 143–165.

Ambraseys, N. (2002), Seismic sea-waves in the Marmara Sea region during the last 20 centuries, *J. Seismol.*, *6*, 1–8.

Ambraseys, N., and A. Zatopek (1969), The Mudurnu valley earthquake of July 22nd 1967, *Bull. Seismol. Soc. Am.*, *59*, 521–589.

Ambraseys, N., and C. Finkel (1995), *The Seismicity of Turkey and Adjacent Areas: A Historical Review, 1500–1800*, pp. 240, Muhittin Salih Eren, Istanbul.

Ambraseys, N., and J. Jackson (1998), Faulting associated with historical and recent earthquakes in the Eastern Mediterranean region, *Geophys. J. Int.*, *133*(2), 390–406.

An, L. Y. (1997), Maximum link distance between strike-slip faults: Observations and constraints, *Pure Appl. Geophys.*, *150*, 19–36.

Anderson, J. G., and J. E. Luco (1983), Consequences of slip rate constraints on earthquake occurrence relations, *Bull. Seismol. Soc. Am.*, *73*, 471–496.

Armijo, R., B. Meyer, A. Hubert, and A. Barka (1999), Westwards propagation of the North Anatolian Fault into the Northern Aegean: Timing and kinematics, *Geology*, *27*, 267–270.

Armijo, R., B. Meyer, S. Navarro, G. King, and A. Barka (2002), Asymmetric slip partitioning in the Sea of Marmara pull-apart: A clue to propagation processes of the North Anatolian Fault?, *Terra Nova*, *14*, 80–86.

Armijo, R., et al. (2005), Submarine fault scarps in the Sea of Marmara pull-apart (North Anatolian Fault): Implications for seismic hazard in Istanbul, *Geochem. Geophys. Geosyst.*, *6*, Q06009, doi:10.1029/2004GC000896.

Atakan, K., A. Ojeda, M. Meghraoui, A. Barka, M. Erdik, and A. Bodare (2002), Seismic hazard in Istanbul following the August 17, 1999 Izmit and November 12, 1999 Düzce earthquakes, *Bull. Seismol. Soc. Am.*, *92*(1), 466–482.

Barka, A. (1999), The 17 August 1999 Izmit earthquake, *Science*, *285*, 1858–1859.

Barka, A. A. (1992), The North Anatolian Fault Zone, *Ann. Tectonicae*, Special Issue, *VI*, 161–195.

Barka, A. A. (1996), Slip distribution along the North Anatolian Fault associated with the large earthquakes of the period 1939 to 1967, *Bull. Seismol. Soc. Am.*, *86*, 1238–1254.

Barka, A., and I. Kuscu (1996), Extends of the North Anatolian Fault in the Izmit, Gemlik and Bandirma Bays, Turkish, *J. Mar. Sci.*, *2*, 93–106.

Barka, A., and K. Kadinsky-Cade (1988), Strike-slip fault geometry in Turkey and its influence on earthquake activity, *Tectonics*, *7*, 663–684, doi:10.1029/TC007i003p00663.

Barka, A., et al. (2002), The surface rupture and slip distribution of the 17 August 1999 Izmit earthquake (*M*7.4), North Anatolian fault, *Bull. Seismol. Soc. Am.*, *92*(1), 43–60.

Bohnhoff, M., H. Grosser, and G. Dresen (2006), Strain partitioning and stress rotation at the North Anatolian fault zone from aftershock focal mechanisms of the 1999 Izmit $M_w = 7.4$ earthquake, *Geophys. J. Int.*, *166*(1), 373–385.

Bohnhoff, M., F. Bulut, G. Dresen, P. E. Malin, T. Eken, and M. Aktar (2013), An earthquake gap south of Istanbul, *Nature*, doi:10.1038/ncomms2999.

Bulut, F., Bohnhoff, M., Aktar, M., and Dresen, G. (2007), Characterization of aftershock-fault plane orientations of the 1999 Izmit (Turkey) earthquake using high-resolution aftershock locations, *Geophys. Res. Lett.*, *34*, L20306, doi:10.1029/2007GL031154.

Bulut, F., M. Bohnhoff, W. L. Ellsworth, M. Aktar and G. Dresen (2009), Microseismicity at the North Anatolian Fault in the Sea of Marmara offshore Istanbul, NW Turkey, *J. Geophys. Res.*, *114*, B09302, doi:10.1029/2008JB006244.

Cakir, Z., A. M. Akoglu, S. Belabbes, S. Ergintav, and M. Meghraoui (2005), Creeping along the Ismetpasa section of the North Anatolian fault (Western Turkey): Rate and extent from InSAR, *Earth Planet. Sci. Lett.*, *238*, 225–234.

Canitez, N. (1972), Source mechanism and rupture propagation in the Mudurnu Valley, Turkey, earthquake of July 22, 1967, *Pure Appl. Geophys.*, *93*(1), 116–124.

Carton, H., et al. (2007), Seismic imaging of the three-dimensional architecture of the Çınarcık Basin along the North Anatolian Fault, *J. Geophys. Res.*, *112*, B06101, doi:10.1029/2006JB004548.

Cattin, R., N. Chamot-Rooke, M. Pubellier, A. Rabaute, M. Delescluse, C. Vigny, L. Fleitout, and P. Dubernet (2009), Stress change and effective friction coefficient along the Sumatra-Andaman-Sagaing fault system after the 26 December 2004 (M_w = 9.2) and the 28 March 2005 (M_w = 8.7) earthquakes, *Geochem. Geophys. Geosyst.*, *10*, Q03011, doi:10.1029/2008GC002167.

Console, R., and F. Catalli (2006), A rate-state model for aftershocks triggered by dislocation on a rectangular fault: a review and new insights, *Ann. Geophys.*, *49*(6), 1259–1263.

Console, R., Murru, M., Falcone, G., and Catalli, F. (2008), Stress interaction effect on the occurrence probability of characteristic earthquakes in Central Apennines, *J. Geophys. Res.*, *113*, B08313, doi:10.1029/2007JB005418.

Console, R., G. Falcone, V. Karakostas, M. Murru, E. Papadimitriou, and D. Rhoades (2013), Renewal models and co-seismic stress transfer in the Corinth Gulf, Greece, fault system, *J. Geophys. Res. Solid Earth*, *118*, 3655–3673, doi:10.1002/jgrb.50277.

Console, R., R. Carluccio, E. Papadimitriou, and V. Karakostas (2014), Synthetic earthquake catalogs simulating seismic activity in the Corinth Gulf, Greece, Fault system, *J. Geophys. Res. Solid Earth*, *120*, 326–343, doi:10.1002/2014JB011765.

Cramer, C. H., M. D. Petersen, T. Cao, T. R. Toppozada, and M. Reichle (2000), A time dependent probabilistic seismic hazard model for California, *Bull. Seismol. Soc. Am.*, *90*(1), 1–21.

Deng, J., and L. R. Sykes (1997a), Stress evolution in southern California and triggering of moderate-, small-, and micro-size earthquakes, *J. Geophys. Res.*, *102*(B11), 24,411–24,435, doi:10.1029/97JB02127.

Deng, J., and L. R. Sykes (1997b), Evolution of the stress field in southern California and triggering of moderate-size Earthquakes: A 200-year perspective, *J. Geophys. Res.*, *102*(B5), 9859–9886, doi:10.1029/96JB03897.

Doğan, B., O. Tuysuz, and F. B. Sanli (2015), Tectonostratigraphic evolution of the basins on the southern branch of the North Anatolian Fault System in the SE Marmara Region, Turkey, *Int. J. Earth Sci.*, *104*(2), 389–418.

Dolu, E., et al. (2007), Quaternary evolution of the Gulf of Izmit (NW Turkey): A sedimentary basin under control of the North Anatolian Fault Zone, *Geo Mar. Lett.*, *27*, 355–381.

Ellsworth, W. L., Matthews, M. V., Nadeau, R. M., Nishenko, S. P., Reasenberg, P. A., Simpson, R. W. (1999), A physically-based earthquake recurrence model for estimation of long-term earthquake probabilities, *Open-File Rep*, *U.S. Geol. Surv.*, Series number: 99-522, 22.

Erdik, M., M. Demircioglu, K. Sesetyan, E. Durukal, and B. Siyahi (2004), Earthquake hazard in Marmara Region, Turkey, *Soil Dyn. Earthquake Eng.*, *24*, 605–631.

Ergintav, S., R. E. Reilinger, R. Cakmak, M. Floyd, Z. Cakir, U. Dogan, R. W. King, S. McClusky, and H. Ozener (2014), Istanbul's earthquake hot spots: Geodetic constraints on strain accumulation along faults in the Marmara seismic gap, *Geophys. Res. Lett.*, *41*, 5783–5788, doi:10.1002/2014GL060985.

Falcone, G., Console R., Murru M. (2010), Short-term and long-term earthquake occurrence models for Italy: ETES, ERS and LTST, *Ann. Geophys.*, *53*, 3, doi:10.4401/ag-4760, *special volume entitled "An earthquake forecast experiment in Italy"* edited by W. Marzocchi, D. Schorlemmer, and S. Wiemer.

Field, E. H., and M. T. Page (2011), Estimating earthquake rupture rates on a fault or fault system, *Bull. Seismol. Soc. Am.*, *101*, 79–92, doi:10.1785/0120100004.

Field, E. H., D. D. Jackson, and J. F. Dolan (1999), A mutually consistent seismic-hazard source model for Southern California, *Bull. Seismol. Soc. Am.*, *89*(3), 559–578.

Field, E. H., et al. (2009), The uniform California earthquake rupture forecast, version 2 (UCERF2), *Bull. Seismol. Soc. Am.*, *99*, 2053–2107, doi:10.1785/0120080049.

Field, E. H., et al. (2014), Uniform California Earthquake Rupture Forecast, Version 3 (UCERF3)—The time-independent model, *Bull. Seismol. Soc. Am.*, *104*, 1122–1180, doi:10.1785/0120130164.

Flerit, F., R. Armijo, G. C. P. King, B. Meyer, and A. Barka (2003), Slip partitioning in the Sea of Marmara pull-apart determined from GPS velocity vectors, *Geophys. J. Int.*, *154*, 1–7, doi:10.1046/j.1365-246X.2003.01899.x.

Flerit, F., R. Armijo, G. King, and B. Meyer (2004), The mechanical interaction between the propagating North Anatolian Fault and the back-arc extension in the Aegean, *Earth Planet. Sci. Lett.*, *224*, 347–362.

Gasperini, L., A. Polonia, M. N. Çağatay, G. Bortoluzzi, and Ferrante, V. (2011), Geological slip rates along the North Anatolian Fault in the Marmara region, *Tectonics*, *30*, TC6001, doi:10.1029/2011TC002906.

Guidoboni, E., and A. Comastri (Eds) (2005), *Catalogue of Earthquakes and Tsunamis in the Mediterranean Area From the 11th to the 15th Century*, pp. 1037, Ist. Naz. di Geophys. e Vulcanol, Bologna, Italy.

Guidoboni, E., A. Comastri, and G. Traina (1994), *Catalogue of Ancient Earthquakes in the Mediterranean Area up to the 10th Century*, pp. 504, Ist. Naz. di Geofis, Rome.

Gülen, L., A. Pinar, D. Kalafat, N. Özel, G. Horasan, M. Yilmazer, and A. M. Işikara (2002), Surface fault breaks, aftershock distribution, and rupture process of the 17 August 1999 Izmit, Turkey, earthquake, *Bull. Seismol. Soc. Am.*, *92*(1), 230–244.

Gülerce, Z., and S. Ocak (2013), Probabilistic seismic hazard assessment of Eastern Marmara Region, *Bull. Earthquake Eng.*, *11*(5), 1259–1277.

Gürbüz, C., et al. (2000), On the seismotectonics of the Marmara region (Turkey): Results from a microseismic experiment, *Tectonophysics*, *316*(1–2), 1–17.

Gutenberg, B., and C. F. Richter (1956), Earthquake magnitude, intensity, energy and acceleration, *Bull. Seismol. Soc. Am.*, *46*, 105–145.

Hagiwara, Y. (1974), Probability of earthquake occurrence as obtained from a Weibull distribution analysis of crustal strain, *Tectonophysics*, *23*, 313–318.

Hanks, T. C., and W. H. Bakun (2008), M-logA observations of recent large earthquakes, *Bull. Seismol. Soc. Am.*, *98*, 490.

Hanks, T. C., and H. Kanamori (1979), A moment magnitude scale, *J. Geophys. Res.*, *84*(B5), 2348–2350, doi:10.1029/JB084iB05p02348.

Harris, R. A., and R. W. Simpson (1998), Suppression of large earthquakes by stress shadows: A comparison of Coulomb and rate-and-state failure, *J. Geophys. Res.*, *103*, 24,439–24,451, doi:10.1029/98JB00793.

Hecker, S., and N. A. Abrahamson (2004), Low slip-at-a-point variability: Implications for earthquake-size distribution, fault rupture hazard, and ground-motion modeling: Basin and range seismic hazards summit II, *Western States Seismic Policy Council, 16–19 May 2004, Program and Abstracts*, 21–22.

Hergert, T., and O. Heidbach (2010), Slip-rate variability and distributed deformation in the Marmara Sea fault system, *Nat. Geosci.*, *3*(2), 132–135.

Hergert, T., O. Heidbach, A. Becel, and M. Laigle (2011), Geomechanical model of the Marmara Sea region—I. 3-D contemporary kinematics, *Geophys. J. Int*, *185*(3), 1073–1089, doi:10.1111/j.1365-246X.2011.04991.x.
Hubert-Ferrari, A., A. Barka, E. Jacques, S. S. Nalbant, B. Meyer, R. Armijo, and G. C. King (2000), Seismic hazard in the Marmara Sea region following the 17 August 1999 Izmit earthquake, *Nature*, *404*(6775), 269–273.
Hubert-Ferrari, A., R. Armijo, G. King, B. Meyer, and A. Barka (2002), Morphology, displacement, and slip rates along the North Anatolian Fault, Turkey, *J. Geophys. Res.*, *107*(B10), 2235, doi:10.1029/2001JB000393.
Imren, C., X. Le Pichon, C. Rangin, E. Demirbag, B. Ecevitoglu, and N. Gorur (2001), The North Anatolian Fault within the Sea of Marmara: A new interpretation based on multi-channel seismic and multibeam data, *EPSL*, *186*, 143–158.
Ishibe, T., K. Satake, S. Sakai, K. Shimazaki, H. Tsuruoka, Y. Yokota, S. Nakagawa, and N. Hirata (2015), Correlation between Coulomb stress imparted by the 2011 Tohoku-Oki earthquake and seismicity rate change in Kanto, Japan, *Geophys. J. Int.*, *201*, 112–134, doi:10.1093/gji/ggv001.
Kagan, Y. Y., and L. Knopoff (1987), Random stress and earthquake statistics: Time dependence, *Geophys. J. R. Astron. Soc.*, *88*, 723–731.
Kalkan, E., P. Gülkan, N. Yilmaz, and M. Çelebi (2009), Reassessment of probabilistic seismic hazard in the Marmara Region, *Bull. Seismol. Soc. Am.*, *99*(4), 2127–2146.
Kanamori, H., and D. Anderson (1975), Theoretical basis of some empirical relations in seismology, *Bull. Seismol. Soc. Am.*, *65*(5), 1073–1095.
Kaneko, Y., Y. Fialko, D. T. Sandwell, X. Tong, and M. Furuya (2013), Interseismic deformation and creep along the central section of the North Anatolian Fault (Turkey): InSAR observations and implications for rate-and-state friction properties, *J. Geophys. Res. Solid Earth*, *118*, 316–331, doi:10.1029/2012JB009661.
Ketin, I. (1969), Kuzey Anadolu Fayi Hakkinda, *Bull. Miner. Res. Explor. Inst. Turk.*, *76*, 1–25.
King, G. C. P., R. S. Stein, and J. Lin (1994), Static stress changes and the triggering of earthquakes, *Bull. Seismol. Soc. Am.*, *84*, 935–953.
King, G. C., A. Hubert-Ferrari, S. S. Nalbant, B. Meyer, R. Armijo, and D. Bowman (2001), Coulomb interactions and the 17 August 1999 Izmit, Turkey earthquake, *C.R. Acad. Sci., Ser. IIA—Earth Planet, Sci.*, *333*(9), 557–569.
Klinger, Y., K. Sieh, E. Altunel, A. Akoglu, A. Barka, T. Dawson, T. Gonzalez, A. J. Meltzner, and T. Rockwell (2003), Paleoseismic evidence of characteristic slip on the western segment of the North Anatolian Fault, Turkey, *Bull. Seismol. Soc. Am.*, *93*, 2317–2332.
Kondo, H., V. Özaksoy, and C. Yıldırım (2010), Slip history of the 1944 Bolu-Gerede earthquake rupture along the North Anatolian fault system: Implications for recurrence behavior of multisegment earthquakes, *J. Geophys. Res.*, *115*, B04316, doi:10.1029/2009JB006413.
Kondorskaya, N. V., and Ulomov, V. I. (1999), Special catalogue of earthquakes of the Northern Eurasia (SECNE). [Available at http://www.seismo.ethz.ch/gshap/neurasia/nordasiacat.Txt.]
Kürçer, A., Ö. Ateş, A. Chatzipetros, and S. Valkaniotis (2008), The Yenice-Gönen active fault (NW Turkey): Active tectonics and palaeoseismology, *Tectonophysics*, *453*, 263–275.
Kurtuluş, C., and M. M. Canbay (2007), Tracing the middle strand of the North Anatolian Fault Zone through the southern Sea of Marmara based on seismic reflection studies, *Geo-Mar. Lett.*, *27*, 27–40, doi:10.1007/s00367-006-0050-2.
Kuşçu, I., M. Okamura, H. Matsuoka, K. Yamamori, Y. Awata, and S. Özalp (2009), Recognition of active faults and stepover geometry in Gemlik Bay, Sea of Marmara, NW Turkey, *Mar. Geol.*, *260*, 90–101.
Laigle, M., A. Becel, B. de Voogd, A. Hirn, T. Taymaz, S. Ozalaybey, and Members of SEISMARMARA Leg1 Team (2008), A first deep seismic survey in the Sea of Marmara: Deep basins and whole crust architecture and evolution, *Earth Planet. Sci. Lett.*, *270*, 168–179.
Le Pichon, X., A. M. C. Şengör, E. Demirbağ, C. Rangin, C. İmren, R. Armijo, N. Görür, and N. Çağatay (2001), The active Main Marmara Fault, *Earth Planet. Sci. Lett.*, *192*, 595–616.
Le Pichon, X., N. Rangin, C. Chamot-Rooke, and A. M. C. Sengör (2003), The North Anatolian Fault in the Sea of Marmara, *J. Geophys. Res.*, *108*(B4), 2179, doi:10.1029/2002JB001862.
Lettis, W., J. Bachhuber, R. Witter, C. Brankman, C. E. Randolph, A. Barka, W. D. Page, and A. Kaya (2002), Influence of releasing stepovers on surface fault rupture and fault segmentation: Examples from the 17 August 1999 Izmit earthquake on the North Anatolian Fault, Turkey, *Seismol. Soc. Am. Bull.*, *92*(1), 19–42.
Matthews, M. V., W. L. Ellsworth, and P. A. Reasenberg (2002), A Brownian model for recurrent earthquakes, *Bull. Seismol. Soc. Am.*, *92*, 2233–2250.
McClusky, S., et al (2000), Global positioning system constraints on plate kinematics and dynamics in the eastern Mediterranean and Caucasus, *J. Geophys. Res.*, *105*(3), 5695–5719, doi:10.1029/1999JB900351.
McKenzie, D. P. (1972), Active tectonics of the Mediterranean region, *Geophys. J. R. Astron. Soc.*, *30*, 109–185.
McKenzie, D. P. (1978), Active tectonics of the Alpine-Himalayan belt: the Aegean Sea and surrounding regions, *Geophys. J. R. Astron. Soc.*, *55*, 217–254.
McNeill, L. C., A. Mille, T. A. Minshull, J. M. Bull, N. H. Kenyon, and M. Ivanov (2004), Extension of the North Anatolian Fault into the North Aegean Trough: Evidence for transtension, strain partitioning, and analogues for Sea of Marmara basin models, *Tectonics*, *3*, 1–12, doi:10.1029/2002TC001490.
Meade, B. J., B. H. Hager, and R. E. Reilinger (2002), Estimates of seismic potential in the Marmara region from block models of secular deformation constrained by GPS measurements, *Bull. Seismol. Soc. Am.*, *92*, 208–215.
Meghraoui, M., M. E. Aksoy, H. S. Akyüz, M. Ferry, A. Dikbaş, and E. Altunel (2012), Paleoseismology of the North Anatolian Fault at Güzelköy (Ganos segment, Turkey): Size and recurrence time of earthquake ruptures west of the Sea of Marmara, *Geochem. Geophys. Geosyst.*, *13*, Q04005, doi:10.1029/2011GC003960.
Middleton, T. A., and A. Copley (2013), Constraining fault friction by re-examining earthquake nodal plane dips, *Geophys. J. Int.*, doi:10.1093/gji/ggt427.
Mogi, K. (1968), Sequential occurrences of recent great earthquakes, *J. Phys. Earth*, *16*, 30–60.
Motagh, M., J. Hoffmann, B. Kampes, M. Baes, and J. Zschau (2007), Strain accumulation across the Gazikoy-Saros segment of the North Anatolian Fault inferred from Persistent Scatterer Interferometry and GPS measurements, *Earth Planet. Sci. Lett.*, *255*(3-4), 432–444, doi:10.1016/j.epsl.2007.01.003.
Muller, J. R., and Aydin, A. (2005), Using mechanical modeling to constrain fault geometries proposed for the northern Marmara Sea, *J. Geophys. Res.*, *110*, B03407, doi:10.1029/2004JB003226.
Nalbant, S. S., A. Hubert, and G. C. P. King (1998), Stress coupling between earthquakes in northwest Turkey and the north Aegean Sea, *J. Geophys. Res.*, *103*(B10), 24,469–24,486, doi:10.1029/98JB01491.
Nishenko, S. P., and R. Buland (1987), A generic recurrence interval distribution for earthquake forecasting, *Bull. Seismol. Soc. Am.*, *77*, 1382–1399.
Noda, H., and N. Lapusta (2013), Stable creeping fault segments can become destructive as a result of dynamic weakening, *Nature*, *493*, 518–21, doi:10.1038/nature11703.

Okay, A. I., E. Demirbağ, H. Kurt, N. Okay, and İ. Kuşçu (1999), An active, deep marine strike-slip basin along the North Anatolian fault in Turkey, *Tectonics*, *18*, 129–148, doi:10.1029/1998TC900017.

Örgülü, G., and M. Aktar (2001), Regional moment tensor inversion for strong aftershocks of the August 17, 1999 Izmit earthquake (M_w = 7.4), *Geophys. Res. Lett.*, *28*(2), 371–374, doi:10.1029/2000GL011991.

Özakın Y., Y. Ben-Zion, M. Aktar, H. Karabulut, and Z. Peng (2012), Velocity contrast across the 1944 rupture zone of the North Anatolian fault east of Ismetpasa from analysis of teleseismic arrivals, *Geophys. Res. Lett.*, *39*, L08307, doi:10.1029/2012GL051426.

Özalaybey, S., M. Ergin, M. Aktar, C. Tapırdamaz, F. Biçmen, and A. Yörük (2002), The 1999 İzmit earthquake sequence in Turkey: Seismological and tectonic aspects, *Bull. Seismol. Soc. Am.*, *92*, 376–386.

Page, M., and K. Felzer (2015), Southern San Andreas Fault seismicity is consistent with the Gutenberg-Richter magnitude-frequency distribution, *Bull. Seismol. Soc. Am.*, *105*, doi:10.1785/0120140340.

Page, M. T., D. Alderson, and J. Doyle (2011), The magnitude distribution of earthquakes near Southern California faults, *J. Geophys. Res.*, *116*, B12309, doi:10.1029/2010JB007933.

Page, M. T., Field, E. H.. Milner, K. R., and P. M. Powers (2013), Appendix N: Grand inversion implementation and testing, *U.S. Geol. Surv. Open-File Rept*. 2013-1165-N, *and California Geol. Surv. Special Rept.* 228-N.

Palyvos, N., D. Pantosti, C. Zabci, and G. D'Addezio (2007), Paleoseismological evidence of recent earthquakes on the 1967 Mudurnu Valley earthquake segment of the North Anatolian Fault Zone, *Bull. Seismol. Soc. Am.*, *97*(5), 1646–1661, doi:10.1785/0120060049.

Pantosti, D., Pucci, S., Palyvos, N., De Martini, P. M., D'Addezio, G., Collins, P. E. F., and Zabci C. (2008), Paleoearthquakes of the Düzce fault (North Anatolian Fault Zone): Insights for large surface faulting earthquake recurrence, *J. Geophys. Res.*, *113*, B01309, doi:10.1029/2006JB004679.

Papazachos, B. C., Scordilis, E. M., Panagiotopoulos, D. G., Papazachos, C. B., and G. F. Karakaisis (2004), Global relations between seismic fault parameters and moment magnitude of earthquakes, *10th Congr. Hellenic Geol. Soc*., Thessaloniki, Greece, 14–17 April 2004, 539–540.

Paradisopoulou, P. M., E. E. Papadimitriou, V. G. Karakostas, T. Taymaz, A. Kilias, and S. Yolsal (2010), Seismic hazard evaluation in Western Turkey as revealed by stress transfer and time-dependent probability calculations, *Pure Appl. Geophys.*, *167*, 1013–1048.

Parsons, T. (2004), Recalculated probability of $M \geq 7$ earthquakes beneath the Sea of Marmara, Turkey, *J. Geophys. Res.*, *109*, B05304, doi:10.1029/2003JB002667.

Parsons, T. (2005), Significance of stress transfer in time-dependent earthquake probability calculations, *J. Geophys. Res.*, *110*, B05S02, doi:10.1029/2004JB003190.

Parsons, T., and E. L. Geist (2009), Is there basis for preferring characteristic earthquakes over Gutenberg-Richter distributions on individual faults in probabilistic earthquake forecasting?, *Bull. Seismol. Soc. Am.*, *99*, 2012–2019, doi:10.1785/0120080069.

Parsons, T., S. Toda, R. S. Stein, A. Barka, and J. H. Dietrich (2000), Heightened odds of large earthquakes near Istanbul: An interaction-based probability calculation, *Science*, *288*, 661–665.

Parsons, T., R. Console, G. Falcone, M. Murru, and K. Yamashina (2012), Comparison of characteristic and Gutenberg-Richter model for time-dependent $M \geq 7.9$ earthquake probability in the Nankai-Tokai subduction zone, Japan, *Geophys. J. Int.*, doi:10.1111/j.1365-246X.2012.05595.x.

Pınar, A., K. Kuge, and Y. Honkura (2003), Moment tensor inversion of recent small to moderate sized earthquakes: Implications for seismic hazard and active tectonics beneath the Sea of Marmara, *Geophys. J. Int.*, *153*, 133–145.

Pondard, N., R. Armijo, G. C. P. King, B. Meyer, and F. Flerit (2007), Fault interactions in the Sea of Marmara pull-apart (North Anatolian Fault): Earthquake clustering and propagating earthquake sequences, *Geophys. J. Int.*, *171*.

Pucci, S., D. Pantosti, M. Barchi, and N. Palyvos (2007), A complex seismogenic shear zone: The Düzce segment of the North Anatolian Fault Zone (Turkey), *Earth Planet. Sci. Lett.*, doi:10.1016/j.epsl.2007.07.038.

Pucci, S., P. M. De Martini, and D. Pantosti (2008), Preliminary slip rates of the Düzce segment of the North Anatolian Fault Zone from offsets geomorphic markers, *Geomorphology*, *97*, 538–554, doi:10.1016/j.geomorph.2007.09.002.

Reid, H. F. (1911), The elastic-rebound theory of earthquakes, *Univ. Calif. Publ. Bull. Dept. Geol. Sci.*, *6*, 413–444.

Reilinger, R. E., S. C. McClusky, and M. B. Oral (1997), GPS measurements of present day crustal movements in the Arabia-Africa-Eurasia plate collision zone, *J. Geophys. Res.*, *102*, 9983–9999, doi:10.1029/96JB03736.

Reilinger, R. E., et al. (2006), GPS constraints on continental deformation in the Africa-Arabia-Eurasia continental collision zone and implications for the dynamics of plate interactions, *J. Geophys. Res.*, *111*, B05411, doi:10.1029/2005JB004051.

Reinecker, J., Heidbach, O., Tingay, M., Connolly, P., and Muller, B. (2004), The 2004 release of the World Stress Map. [Available at www.world-stress-map.org.]

Rikitake, T. (1974), Probability of an earthquake occurrence as estimated from crustal strain, *Tectonophysics*, *23*, 299–312.

Rockwell, T. K., S. Lindvall, T. Dawson, R. Langridge, W. Lettis, and Y. Klinger (2002), Lateral offsets on surveyed cultural features resulting from the 1999 Izmit and Düzce earthquakes, Turkey, *Bull. Seismol. Soc. Am.*, *92*(1), 79–94.

Rockwell, T., A. Barka, T. Dawson, K. Thorup, and S. Akyuz (2001), Paleoseismology of the Gaziköy-Saros segment of the North Anatolia fault, northwestern Turkey: Comparison of the historical and paleoseismic records, implications of regional seismic hazard, and models of earthquake recurrence, *J. Seismol.*, *5*(3), 433–448.

Saroglu F., Emrë O., and Kuscu I. (1992), Turkiye Diri Fay Haritası (Active Fault Map of Turkey), scale 1:2,000,000, one sheet. Maden Tetk, Arama Genel Mudurlugu, Ankara.

SCEC Phase II (1994), Seismic Hazards in Southern California: Probable Earthquakes, 1994 to 2024, *Southern California Earthquake Center, Report*.

Schwartz, D. P., and K. J. Coppersmith (1984), Fault behavior and characteristic earthquakes: Examples from the Wasatch and San Andreas fault zones, *J. Geophys. Res.*, *89*, 5681–5698, doi:10.1029/JB089iB07p05681.

Segall, P., and D. D. Pollard (1980), Mechanics of discontinuous faults, *J. Geophys. Res.*, *85*, 4337–4350, doi:10.1029/JB085iB08p04337.

Selim, H. H., and O. Tüysüz (2013), The Bursa-Gönen Depression, NW Turkey: A complex basin developed on the North Anatolian Fault (NAF), *Geol. Mag.*, *150*(5), 801–821, doi:10.1017/S0016756812000945.

Selim, H. H., O. Tüysüz, A. Karakas, and K. Ö. Tas (2013), Morphotectonic evidence from the southern branch of the North Anatolian Fault (NAF) and basins of the south Marmara sub-region, NW Turkey, *Quaternary Int.*, *292*, 176–192.

Sengör, A. M. C., O. Tüysüz, C. İmren, M. Sakınç, H. Eyidoğan, N. Görür, X. Le Pichon, and C. Rangin (2005), The North Anatolian fault: a new look, *Annu. Rev. Earth Planet. Sci.*, *33*, 37–112, doi:10.1146/annurev.earth.32.101802.120415.

Shaw, B. E. (2009), Constant stress drop from small to great earthquakes in magnitude-area scaling, *Bull. Seismol. Soc. Am.*, *99*, 871, doi:10.1785/0120080006.

Shaw, B. E. (2013), Earthquake surface slip-length data is fit by constant stress drop and is useful for seismic hazard analysis, *Bull. Seismol. Soc. Am.*, *103*, 876, doi:10.1785/0120110258.

Stein, R., A. Barka, and J. Dieterich (1997), Progressive failure on the North Anatolian fault since 1939 by earthquake stress triggering, *Geophys. J. Int.*, *128*, 594–604.
Stein, S., and A. Newman (2004), Characteristic and uncharacteristic earthquakes as possible artifacts: Applications to the New Madrid and Wabash seismic zones, *Seismol. Res. Lett.*, *75*, 173–187.
Stierle, E., M. Bohnhoff, and V. Vavryčuk (2014), Resolution of non-double-couple components in the seismic moment tensor using regional networks—II: Application to aftershocks of the 1999 Mw 7.4 Izmit earthquake, *Geophys. J. Int.*, *196*(3), 1878–1888.
Straub, C., H.-G. Kahle, and C. Schindler (1997), GPS and geological estimates of the tectonic activity in the Marmara Sea region, NW Anatolia, *J. Geophys. Res.*, *102*, 27,587–27,601, doi:10.1029/97JB02563.
Taymaz, T., H. Eyidogan, and J. Jackson (1991), Source parameters of large earthquakes in the East Anatolian Fault Zone (Turkey), *Geophys. J. Int.*, *106*(3), 537–550.
Tibi, R., G. Bock, Y. Xia, M. Baumbach, H. Grosser, C. Milkereit, S. Karakisa, S. Zünbül, R. Kind, and J. Zschau (2001), Rupture processes of the 1999 August 17 Izmit and November 12 Düzce (Turkey) earthquakes, *Geophys. J. Int.*, *144*(2), F1–F7, doi:10.1046/j.1365-246x.2001.00360.x.
Utkucu, M., S. S. Nalbant, J. McCloskey, S. Steacy, and O. Alptekin (2003), Slip distribution and stress changes associated with the 1999 November 12, Düzce (Turkey), *Geophys. J. Int.*, *153*, 229–241.
Utsu, T. (1972a), Large earthquakes near Hokkaido and the expectancy of the occurrence of a large earthquakes off Nemuro, *Report of the Coordinating Committee for Earthquake Prediction*, 7, 7–13.
Utsu, T. (1972b), Aftershocks and earthquake statistics (IV), *J. Fac. Sci. Hokkaido Univ., Ser. VII*, *4*, 1–42.
Vardar, D., K. Öztürk, C. Yaltırak, B. Alpar, and H. Tur (2014), Late Pleistocene-Holocene evolution of the southern Marmara shelf and sub-basins: Middle strand of the North Anatolian fault, southern Marmara Sea, Turkey, *Mar. Geophys. Res.*, doi:10.1007/s11001-013-9210-8.
Weldon, R. J., Schmidt, II, D. A., Austin, L. J., Weldon, E. M., and T. E. Dawson (2013), Appendix D: Compilation of creep rate data for California faults and calculation of moment reduction due to creep, *U.S. Geol. Surv. Open-File Rept. 2013-1165-D, and California Geol. Surv. Special Rept. 228-D*.
Wells, D. L., and K. J. Coppersmith (1994), Empirical relationships among magnitude, rupture length, rupture width, rupture area, and surface displacement, *Bull. Seismol. Soc. Am.*, *84*, 974–1002.
Wesnousky, S. G. (1988), Seismological and structural evolution of strike-slip faults, *Nature*, *335*, 340–343.
Wesnousky, S. G. (1994), The Gutenberg-Richter or characteristic earthquake distribution, which is it?, *Bull. Seismol. Soc. Am.*, *84*, 1940–1959.
WGCEP (Working Group on California Earthquake Probabilities) (1995), Seismic hazards in Southern California: probable earthquakes, 1994 to 2024, *Bull. Seismol. Soc. Am.*, *85*, 379–439.
WGCEP (Working Group on California Earthquake Probabilities) (2003), Earthquake probabilities in the San Francisco Bay region: 2002 to 2031, *Open-File Rep*, U.S. Geol. Surv., 03–214.
WGCEP (Working Group on California Earthquake Probabilities) (2008), The Uniform California Earthquake Rupture Forecast, Version 2 (UCERF 2), *U.S. Geological Survey Open-File Report 2007-1437 and California Geological Survey Special Report 203*.
Woessner, J., Jónsson, S., Sudhaus, H., and Baumann, C. (2012), Reliability of Coulomb stress changes inferred from correlated uncertainties of finite-fault source models, *J. Geophys. Res.*, *117*, B07303, doi:10.1029/2011JB009121.
Wong, H. K., T. Lüdmann, A. Ulug, and N. Görür (1995), The Sea of Marmara: A plate boundary sea in an escape tectonic regime, *Tectonophysics*, *244*, 231–250.
Woodcock, N., and M. Fischer (1986), Strike-slip duplexes, *J. Struct. Geol.*, *8*, 725–735.
Yaltirak, C. (2002), Tectonic evaluation of Marmara Sea and its surroundings, *Mar. Geol.*, *190*, 439–529.
Zabcı, C., H. S. Akyüz, V. Karabacak, T. Sançar, E. Altunel, H. Gürsoy, and O. Tatar (2011), Palaeoearthquakes on the Kelkit Valley segment of the North Anatolian Fault, Turkey: Implications for the surface rupture of the historical 17 August 1668 Anatolian earthquake, *Turkish J. Earth Sci*, *20*(4), 411–427.